UiT The Arctic University of Norway

Department of Arctic and Marine Biology

Ageing and growth of the Arctic brittle star *Ophiopleura borealis* (Echinodermata: Ophiuroidea) from the Barents Sea and North East Greenland

Hanna Dinevik

Master's thesis in Biology BIO-3960 May 2024

Table of Contents

List of Tables

List of Figures

Acknowledgements

I want to thank my supervisors, Bodil Bluhm and Andreas Altenburger, for their support, inspiring guidance and of course, for giving me the opportunity to plan and conduct this project. I also want to thank Joel Vikberg Wernström and Vanessa Pitusi at the Arctic University Museum of Norway, for showing me around the lab and answering all my questions, and Fredrik Broms for letting me use one of his photos for the thesis front page. This project would also not have been possible without the ERASMUS programme facilitating my exchange studies at UiT The Arctic University of Norway, or funding from The Nansen Legacy (#276730) to which this project contribute in Work Package 3 The Living Barents Sea. I am also grateful for Raphaelle Descoteaux for collecting the Barents Sea specimens, and Ivan Cautain together with the TUNU benthos team for collecting the Greenland specimens.

I want to thank all my friends, new and old ones, and my family for supporting me wherever in the world I might be.

Abstract

Species inhabiting cold-water environments exhibit typically slower growth and a longer lifespan than warm-water species, implying a slowed ability to recover from natural and anthropogenic disturbances. Longevity estimates for species inhabiting the Arctic region are sparse, despite the ongoing changes and disturbances in the region.

Brittle stars (Ophiuroidea) often dominate Arctic shelf epibenthic communities, impacting biogeochemical fluxes and sediment structure. Assessing their resilience to disturbances relies on estimates of their longevity. However, only a handful of studies on brittle star age are available, including three on Arctic species.

In this study, I showed that growth bands similar to those seen in the arm bones of other brittle star species were also present in *O. borealis* specimens from North East Greenland and the Barents Sea. By counting the growth bands using scanning electron microscopy (SEM) and correcting the count for overgrown bands, ages could be estimated in 80 individuals as growth bands are likely formed annually. The maximum age estimated was 39 years, which is the first longevity estimate to be presented for *O. borealis*.

The Specialized von Bertalanffy, the Gompertz and the Single Logistic growth functions were applied to the age data to construct growth curves. The growth constants estimated by each model indicated the growth of *O. borealis* to be similar to that of other polar brittle stars.

These results contribute to information on the longevity of an Arctic benthic invertebrate – which can be applied when estimating impacts of disturbances on the species and, consequently, the Arctic benthic ecosystem.

1 Introduction

The Arctic encompasses the northernmost habitats of the Earth, where both terrestrial and marine organisms have adapted to extreme conditions and strong seasonality. The Arctic seafloor was once considered a “poor” habitat with populations exhibiting low productivity and diversity, however, this notion has been disproven in the last decades (Piepenburg, 2005). Despite research highlighting the major role the Arctic benthic fauna play in ecosystem processes, this role is far from being fully understood (Piepenburg, 2005). It is no secret either, that the Arctic marine ecosystem is undergoing rapid changes due to climate change and anthropogenic stressors (Intergovernmental Panel on Climate Change (IPCC), 2022; Ivanova et al., 2020), with no exception for the benthos (Grebmeier et al., 2006; Kortsch et al., 2012). Studies point to both ongoing and future changes in the Arctic benthic community structure, biogeography and ecosystem functioning (Al-Habahbeh et al., 2020; Frainer et al., 2017; Kortsch et al., 2012; Morata et al., 2020). Information on how resilient, or vulnerable, benthic species are to different stressors and disturbances is needed in order to facilitate a sustainable management of the Arctic region.

Longevity and growth rates have been connected to the vulnerability of a species, with slow-growing marine invertebrates may needing decades to recover from disturbances (Neves et al., 2015). Slow growth and high longevity on the order of decades being typical for organisms in high-latitude and cold-water environments (Bluhm et al., 1998; Ravelo et al., 2017). It is not unexpected then, that differences in recovery rates have been observed across latitudes (Al-Habahbeh et al., 2020), and it could indicate an increased vulnerability in polar organisms.

With more than 2000 species described worldwide, brittle stars (Ophiuroidea) make up the largest living group of echinoderms (Stöhr et al., 2012). These epibenthic organisms are found in all marine environments, often hidden in the upper sediment layers of the seafloor and in various crevices, with some species being epizoic (Stöhr et al., 2012).

Brittle stars play important roles in the ecosystem. Apart from being prey to many crab- and fish species (Burukovsky et al., 2021; Freire & González-Gurriarán, 1995; Hinz et al., 2005; Hüssy et al., 2016; Rowe & Smith, 2022), as well as to other echinoderms (Drolet et al., 2004; Gaymer et al., 2004), brittle stars can affect their environment considerably. They are known to aggregate (Broom, 1975; Calero et al., 2018; Fujita & Ohta, 1989) and in extreme cases

can cover the seabed with more than 7000 individuals per square meter (Davoult & Migné, 2001). Previous studies have found that aggregations of brittle stars can affect biogeochemical fluxes (Davoult m.fl., 2009; Wood m.fl., 2009) and sediment structure- and oxygen supply (Broach m.fl., 2016; Murat m.fl., 2016; Vopel, 2003). This arguably make brittle stars fit the description of ecosystem engineers (Jones m.fl., 1994). Studies have also indicated suspension feeding brittle star species to play an important role in nutrient cycling and benthic-pelagic coupling (Dauvin et al., 2013; Geraldi et al., 2016).

There are relatively few species of brittle stars in the Arctic compared to other regions where the number of species are in the hundreds (Stöhr et al., 2012). In the comprehensive review on global diversity of brittle stars, Stöhr et al. (2012) reported that there are 73 brittle star species in the Arctic (defined as above 60°N in the review). Brittle stars are, however, described as one of the dominating groups in epibenthic communities on the Arctic shelves in terms of both biomass and abundance (Piepenburg et al., 1997; Piepenburg & Schmid, 1996; Ravelo et al., 2014, 2017). For example, Piepenburg & Schmid (1996) have reported median abundances of up to 524 individuals per square meter in study areas in the Barents Sea, while Ravelo et al. (2014) found that ophiuroids accounted for up to 71% of the average abundance of epibenthos in the Chukchi Sea.

Ophiopleura borealis (Danielssen & Koren, 1877) (Fig. 1) is an endemic brittle star species common in the Arctic (Piepenburg & Schmid, 1996; Udalov et al., 2018; Yunda-Guarin et al., 2022; Zhulay et al., 2019), where the bathymetric distribution range of the species is from 40 m to 1400 m (Piepenburg, 2000). While little is known about its life history, *O. borealis* has been described as a large-bodied (disc diameter > 4 cm) scavenger and deposit feeder (Gallagher et al., 1998; Piepenburg & von Juterzenka, 1994). Several reproduction modes have been observed in ophiuroids including broadcast spawning and brooding (Stöhr et al., 2012), however it has been suggested that *O. borealis* has a pelagic stage as an ophiopluteus larva due to its small eggs (Piepenburg & von Juterzenka, 1994).

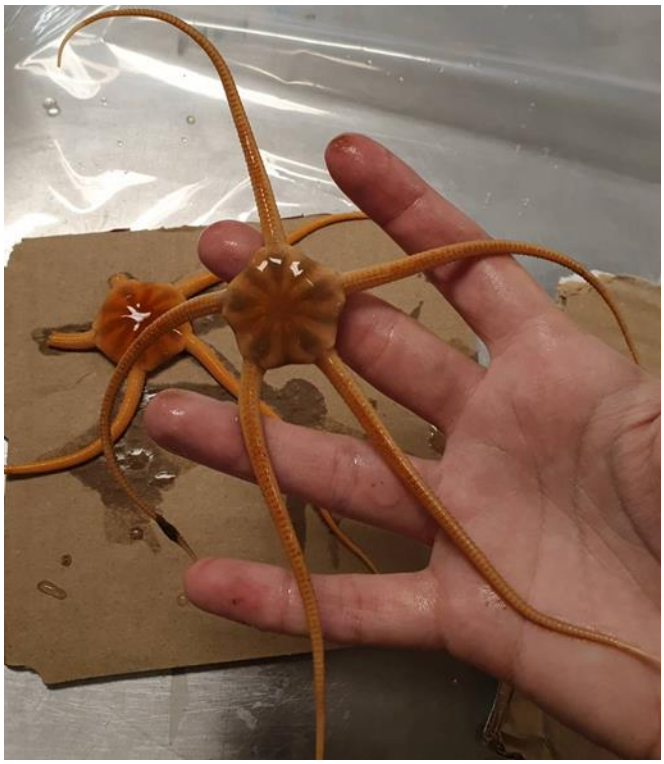

Figure 1. Ophiopleura borealis *caught off the Svalbard coast.*

Out of the handful of studies on brittle star age conducted so far (Dahm, 1993; Gage, 1990b, 2003; Orino et al., 2019), three have focused on brittle star ages in the Arctic (Ravelo et al., 2017; Stratanenko, 2021; Stratanenko & Denisenko, 2020), yielding maximum age estimates from eight to 27 years.

In seasonal systems such as the Arctic, growth patterns have been observed in the skeletal elements of echinoderms which have been utilized to obtain age estimations (Brey et al., 1995; Gage, 1992; Sun et al., 2019). The brittle star skeleton consists of a magnesium-calcite meshwork called stereom (Stöhr et al., 2012), resulting in hard structures constituting an exo- and endoskeleton. The endoskeleton includes the arm bones which are called the vertebrae. Similar to a backbone, the vertebrae consist of "stacked" discs referred to as ossicles (Fig. 2) in which growth patterns have been observed and connected to changes in growth rate over time (Gorzula, 1977; Orino et al., 2019; Ravelo et al., 2017). The further away an ossicle is positioned from the disc, the younger it is (Stöhr et al., 2012), especially if the arm in question have been broken and regenerated. The study of growth patterns in ossicles and other hard structures in organisms have, however, been in practice for a long time. Stemming from dendrochronology, sclerochronology refers to the study of physical and chemical variations in

the hard structures of an organism (Oschmann, 2009). The term was originally applied in research on age and growth rates in corals in the 1970's (Buddemeier et al., 1974; Hudson et al., 1976), but the idea of obtaining information on an organism from its hard structures can be traced back centuries (Leeuwenhoek, 1685; Pulteney, 1781; Whitfield, 1898). Today, sclerochronological methods are often paired with different chemical analyses (Peharda et al., 2022) and are utilized in a wide array of fields such as paleontology, archaeology and ecology in order to learn about organisms life histories, reconstruct past climate and more (Abdelhady et al., 2024; Andrus et al., 2024; Roman Gonzalez, 2021).

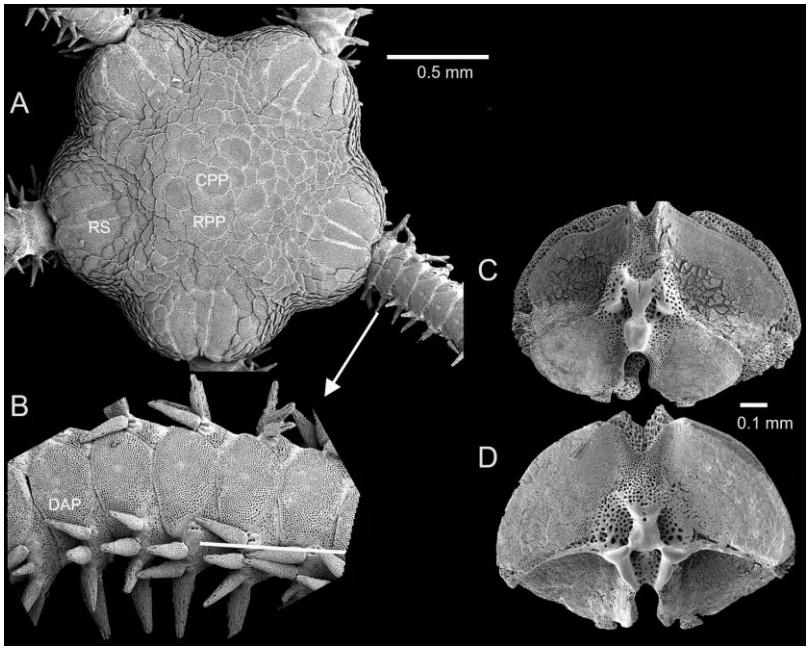

Figure 2. Skeletal morphology of a brittle star vertebrae, shown on Amphiura chaijei*. (A) aboral disc side, (B) segmented arm exterior, (C) distal side of ossicle (i.e. facing away from the disc), (D) proximal side of ossicle (i.e. facing towards the disc). Image modified from Stöhr et al (2012).*

In this study, ages of *O. borealis* specimens from Greenland and the Barents Sea are inferred, in order to provide much needed information on growth and longevity for this common species inhabiting the Arctic seafloor. This study provides the first age estimates for *O. borealis* and information on the longevity of an Arctic benthic invertebrate – which can be applied when anticipating the effects of disturbances on the species and, consequently, the Arctic benthic ecosystem.

2 Objectives and hypotheses

The main objective for this study is to provide age- and growth data on the *Ophiopleura borealis* specimens collected in the Arctic. In addition to this the following hypotheses will be tested:

1) Growth bands similar to those described in previous studies will be visible on the vertebrae ossicle surfaces.

2) *O. borealis* exhibits slower growth compared to brittle star species from lower latitudes.

3) The maximum age of the *O. borealis* specimens will exceed known ages for brittle stars from lower latitudes.

3 Methods

3.1 Collection of brittle stars

The majority of specimens of *Ophiopleura borealis* were collected from northern the Barents Sea (figure 1) in November 2017 onboard R/V Helmer Hanssen as part of the Arctic PRIZE project (*Arctic PRIZE — Scottish Association for Marine Science, Oban UK*), and in August 2018 onboard R/V Kronprins Haakon as part of the Nansen Legacy Project (Ingvaldsen et al., 2020).

In 2017, specimens were collected at 167 m depth at station B4, 77.46183°N 27.629693°E (Fig. 3), using a 2 m beam trawl with a mesh size of 25 mm and 4 mm in the cod-end. The trawl was towed at a speed of 1.5 knots for 3 minutes on the seafloor. The catch was then subsampled, sorted by taxa, and identified down to the lowest taxonomic level possible using a photographic guide to the Barents Sea trawl fauna provided by Lis Jørgensen at the Institute of Marine Research onboard. Specimens of *Ophiopleura borealis* were then frozen in plastic bags at -20 ℃.

In 2018 additional specimens were collected using a Campelen 1800 trawl with 8 mm mesh size in the cod-end, at 284 m depth (station P3/NLEG07, 78.8231°N 34.2506°E, Fig. 3). The

trawl was deployed for 15 minutes on the seafloor at 3 knots and the catch was processed as described above.

Due to few small specimens being available from the Barents Sea collection, these were supplemented with specimens from a collection from the Northeast Greenland shelf. In August 2022, specimens of *O. borealis* were collected off the coast of Northeast Greenland (Fig. 3) onboard R/V Kronprins Haakon as part of the TUNU programme (*TUNU - Biodiversity and Ecology of NE Greenland biota*). The same Campelen trawl 1800 used in the Barents Sea was deployed at 447 m depth (Besselfjord C station 5, 75.977°N 20.313°W) for 10 minutes at 3 knots. The latitude was close to that from station B4 in the Barents Sea.

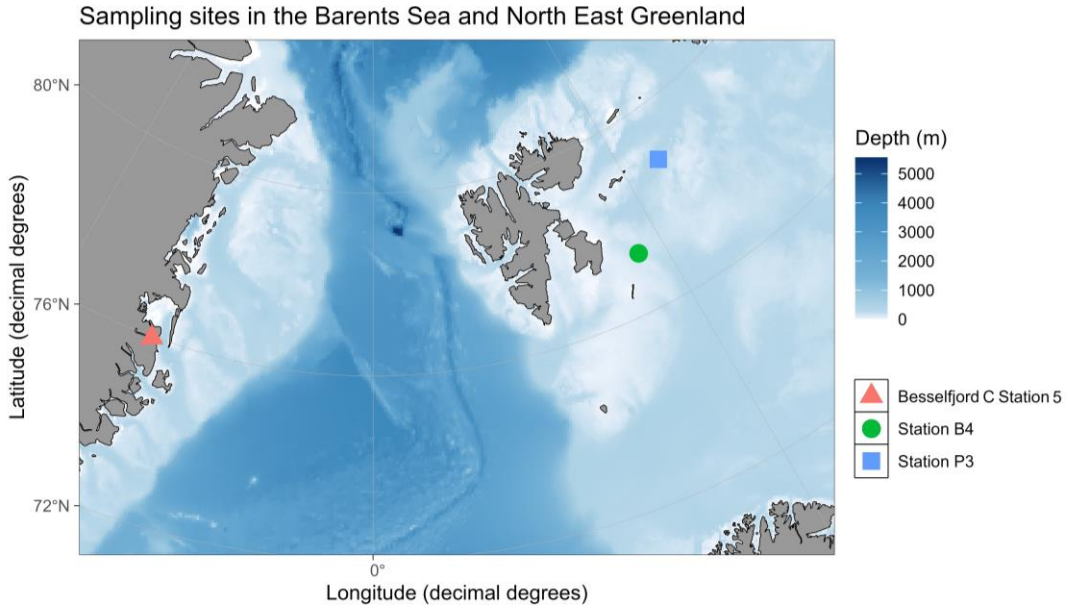

Figure 3. Sampling sites in the Barents Sea stations B4 and P3, and in North East Greenland station 5 ("Besselfjord C Stations 5" in figure).

3.2 Body measurements and preparation of ossicles

A total of 142 specimens of *O. borealis* were picked out from the Barents Sea samples so that all disc sizes would be represented. Since few small specimens were found, an additional 36 individuals were later picked from the North East Greenland sample.

The frozen specimens were thawed in a sealed container in a 60°C-water bath for 10-20 minutes, depending on the size of the specimens. Following 10 minutes of drying on paper towels, specimens were assigned individual numbers before being photographed aboral side

up (Fig. 4a) using a Sony A7 III digital camera. Photographs were taken on top of a mat marked with 1x1 cm squares and included a graph paper with 0.5x0.5 cm squares as well. The known distances were later used for the calibration of mm in the digital images.

For each specimen, the disc diameter (DD) was measured up to three times from the base of one arm to the opposite disc edge (Fig. 4b), to obtain a mean DD. Due do disc damage in five specimens, the mean DD in four of the specimens was calculated from less disc measurements, while the disc was too damaged in one specimen to measure at all. The latter specimen was therefore excluded from the DD dataset.

Based on the smallest and largest DDs recorded for the Barents Sea specimens, individuals were divided into 7 size groups (0.5-1 cm, 1-1.5 cm, 1.5-2 cm, 2-2.5 cm, 2.5-3 cm, 3-3.5 cm, 3.5-4 cm and >4 cm) to ensure a near-homogeneous representation of differently sized brittle stars in the final data.

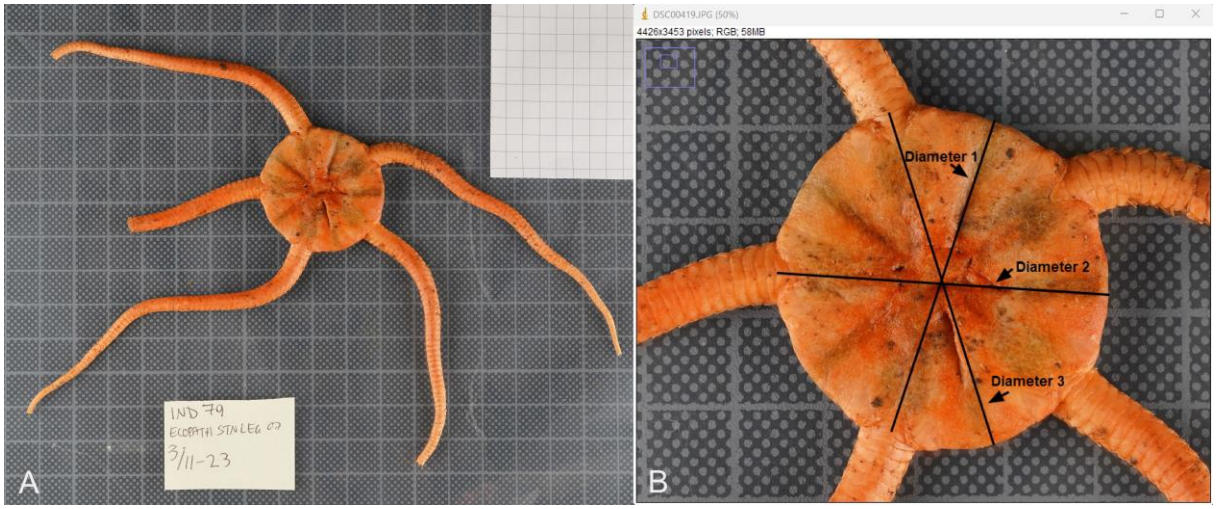

Figure 4. (A) showing how individuals of Ophiopleura borealis *were photographed. (B) illustration how disc diameter was measured in ImageJ software.*

Except for individuals 1-9, the disc of each brittle star was weighed after the arms had been cut off by the disc edge. For disc- and arm weights above 2 g, a 0.1 g resolution scale was used. For discs weighing below 2 g, a 0.00001 g resolution analytical scale was used.

Individuals were then dissected to remove the ossicle closest to the jaws in each arm (Fig. 5). The remaining tissue was removed following a procedure described by Ravelo et al. (2017): ossicles were submerged in 4-16% sodium hypochlorite in vials, which were then placed in a 60°C-water bath for 10-20 minutes. Vials containing the smallest ossicles, approximately less than 1.5 mm wide, were excluded from the water bath and only subjected to room

temperature. The ossicles were then washed three times in MilliQ water. A final wash with 70% ethanol was added to the procedure, as described by Dahm (1993) and Orino et al. (2019), before drying the ossicles on paper towels.

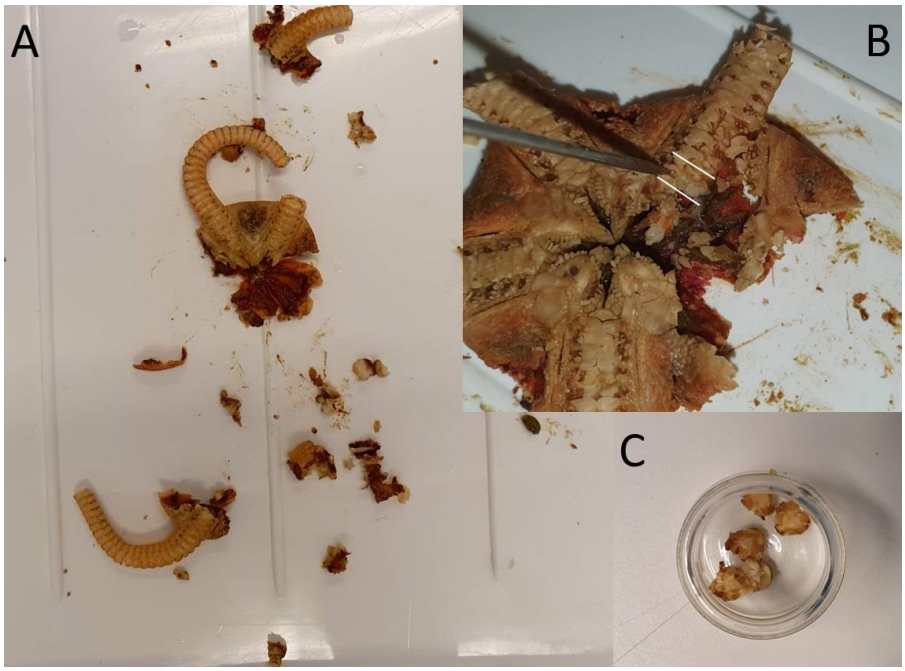

Figure 5. Collage of the dissection of Ophiopleura borealis *individual 3. (A) showing the full body mid-process with oral side up. (B) showing the ossicle (between the two white lines) nearest to the jawbone. (C) showing five ossicles before tissue removal.*

3.3 Image acquisition with Scanning Electron Microscopy

Ossicles were mounted on aluminum pin stubs (12.7 mm diameter) from the company Micro to Nano using conductive carbon tape, and sputter coated in gold for 2x15 second cycles in a JEOL JFC-1300 auto fine coater. Whether the ossicles were mounted with the proximal or distal surface visible was not taken into consideration. The first few ossicles were coated for 1-3x15 second cycles in order to establish how much coating was needed for the ossicles' features to be clearly visible in the Scanning Electron Microscope (SEM). The SEM used was a JEOL NeoScope JCM-7000, in which the diameter of each ossicle was measured horizontally at its widest point (Fig. 6). In the SEM, each ossicle was photographed three times: one photo showing the whole ossicle and two photos showing only the upper left and right fossae (Fig. 6).

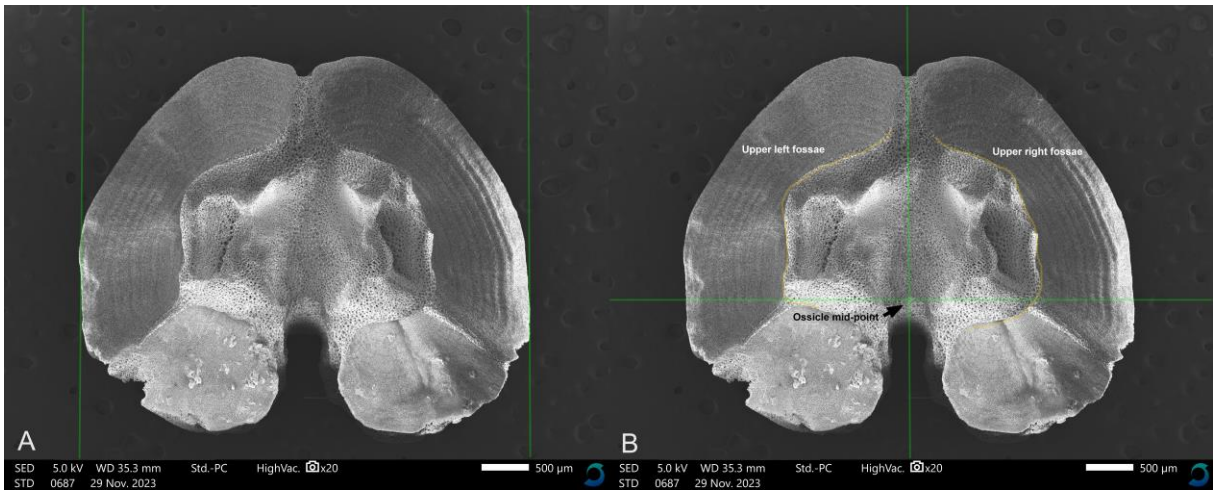

Figure 6. SEM image of an ossicle. (A) the vertical green lines show the distance between the widest points of the ossicle. (B) the areas of the upper fossae are shown above the horizontal green line, as well as the ossicle midpoint and the articulating area outlined in yellow.

Ossicles from 85 individuals were photographed in the SEM to acquire images from about 10 individuals per size group. A larger sample size was not possible in the available time frame. In groups 0.5-1 cm and >4 cm, less than 10 individuals were available, however. Individuals were chosen in no particular order, but those with at least three intact ossicles available were favoured. Ossicles from a few extra individuals were photographed in each size group when available, in case images from any individual turned out to be unfit for image analysis. Images were deemed unfit if damage, remaining tissue or low focus in images rendered the ossicle growth bands unreadable.

In the SEM images, areas of the ossicles were at times obscured by charging artefacts (Fig. 7), likely due to the gold coating not covering the ossicles properly. This was resolved by lowering the accelerating voltage in the SEM from 15 to 5 kV. In some images however, a small amount of white noise was accepted provided it did not obscure the upper fossae.

Figure 7. Example of charging artefacts (the white horizontal line) obscuring part of an Ophiopleura borealis *ossicle in an SEM image at 15 kV.*

3.4 Image analysis

SEM images of ossicles from 80 individual brittle stars were analyzed in ImageJ (Schneider et al., 2012). Five individuals were excluded due to low visibility of growth bands. The aim was to analyze three ossicles per individual, however in some individuals only one or two ossicles were analyzed. Ossicles would sometimes get lost or damaged during dissection. Generally, the smaller an individual was, the more fragile the ossicles were.

3.4.1 Recording growth bands

Growth bands were recorded on the upper left and right fossa in ossicles by marking and numbering each band in ImageJ. A growth band consisted of two adjacent streaks of different stereom densities, often visible as dark and light streaks alternating on the fossa surface (Ravelo et al., 2017), sometimes with ridges associated (Dahm, 1993; Gage, 1990, 2003; Orino et al., 2019). The density changes were assumed to correspond to variation in growth over seasons, as seen and validated in sclerochronological studies of other echinoderms from areas with expressed seasons (Brey et al., 1995; Gage, 1992; Sun et al., 2019). This makes it very likely that one growth band corresponds to one year of growth in the present study.

3.4.2 Age correction

The articulating middle part of ossicles is known to expand as the animal grows, obscuring the inner bands of the fossae (Dahm & Brey, 1998). To correct for growth bands covered by this overgrowth, a procedure similar to that used by Ravelo et al (2017) was applied as follows: the distance from the ossicle midpoint (MP) to the outer edge of the first visible band (VB1) was measured (Fig. 8) in a given ossicle in as close to a ±45° angle as possible. This distance would indicate the number of bands hidden by the overgrowth, once a baseline of distances corresponding to a known number of bands was established. The baseline was constructed by measuring the distance from the MP of a given ossicle to the outer edge of each visibled band (VB) in individuals with the clearest bands (Fig. 8). The largest mean distance of MP to VB1 in the analyzed ossicles was 2.58 mm, which meant that the baseline needed to include bands with a distance to the MP under 2.58 mm.

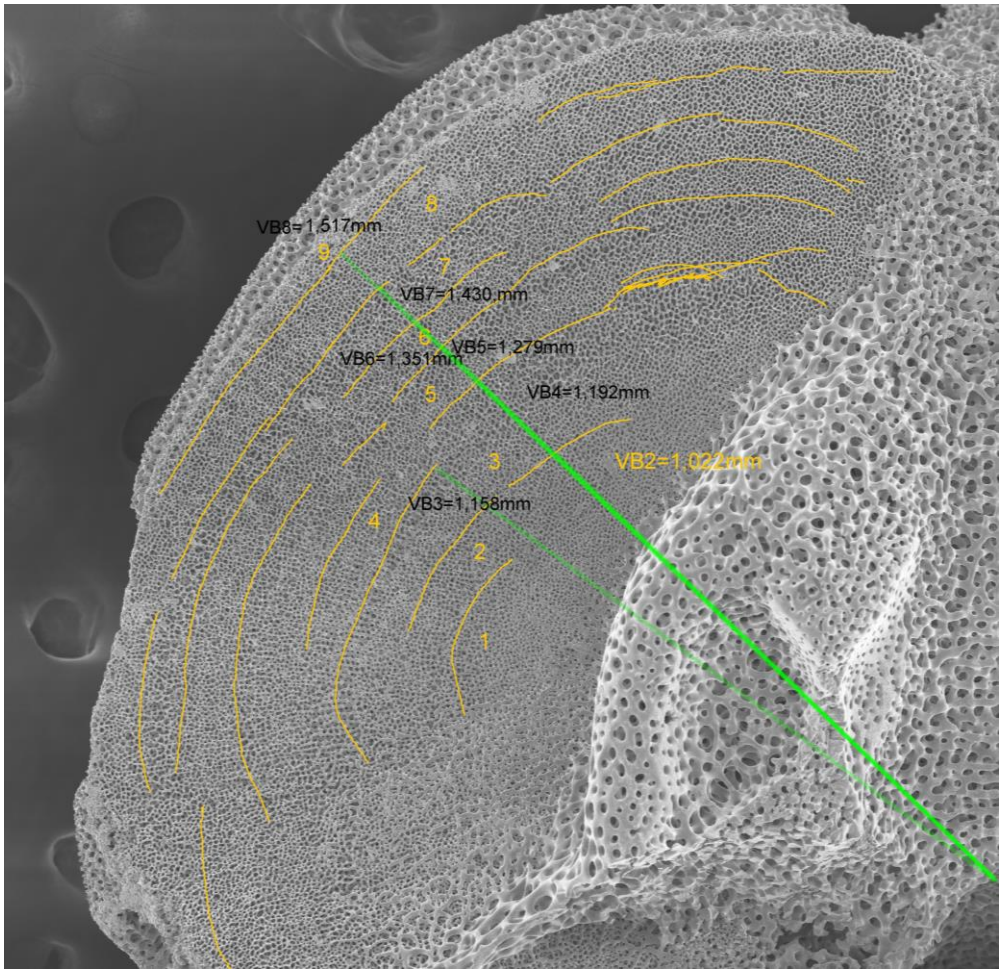

Figure 8. SEM-image showing green lines in approximate -45° angles measures the distance from ossicle midpoint to the outer edge of each visible growthband (VB2, VB3, VB4 and so on). Note that VB9 does not have a marked outer edge, which is why an MP-VB9 distance could not be measured. Distance to VB1 was measured in another image.

The individuals in the smallest size group (0.5-1 cm) were assumed to have no or minimal overgrowth such that no growth bands were obscured. The distance between MP and each growth band was measured in these individuals, arriving at mean MP- to- band distances for up to six growth bands. These distances would constitute baseline intervals for the first six bands (B1-B6), of which some or all would be overgrown in larger individuals. This was repeated using successivley larger individuals until mean distances from MP- to- bands up to 2.58 mm had been established.

A correction factor could then be applied to any ossicles where the MP-VB1 distance exceeded the values for the first band interval established by the baseline measurements. For example, the mean distances between MP-B3 and MP-B4 measured 0.72 mm and 0.78 mm respectively on the baseline. This meant that in an ossicle with a MP-VB1 distance of 0.75 mm, four bands would be hidden by overgrowth (Fig. 9). The number of hidden bands in a given individual would then be added to the initial count of visible bands. The final sum was assumed to correspond to the number of years and is referred to as the corrected age of the individual.

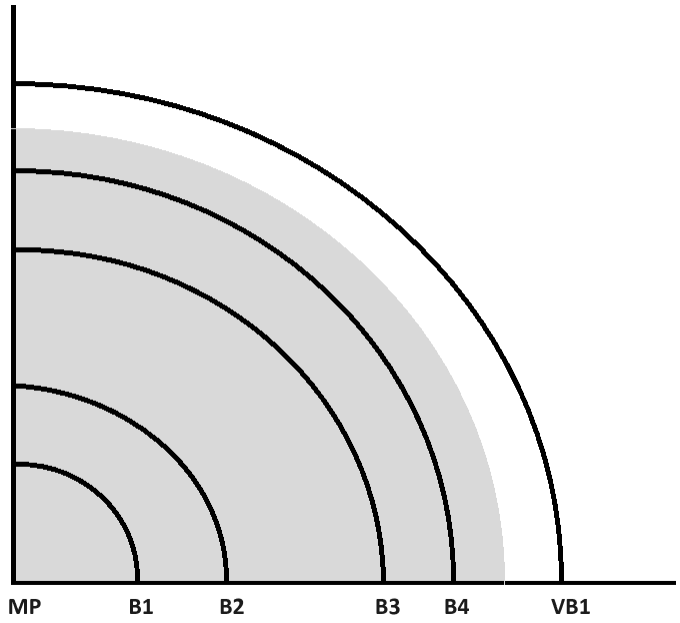

Figure 9. Schematic example showing obscured growth bands in a brittle star ossicle. The shaded area represents the articulating area, or overgrowth, on one of the ossicle fossae. VB1 is the first visible band in this example ossicle. The baseline measurements established the distance of the first growth bands from the ossicle midpoint (MP), such that the MP-VB1 distance in any given ossicle could be corrected for by the number of obscured bands. Here, VB1 is within the baseline interval corresponding to B5, meaning that 4 bands are assumed to be hidden. The number of hidden bands would then be added to the number of visible bands, and the total number of bands interpreted as age in years.

The number of hidden bands in a given individual would then be added to the initial count of visible bands. The final sum was assumed to correspond to number of years, as is referred to as the corrected age of the individual.

3.5 Data analysis

Apart from mean values which were calculated in Microsoft Excel, all data analysis and plotting was conducted using the statistical software R (R Core Team, 2023) with R-packages ggpmisc (Aphalo, 2023), ggplot2 (Wickham, 2016), ggOceanMaps (Vihtakari, 2024), ggpubr (Kassambara, 2023), minpack.lm (Elzhov et al., 2023), magrittr (Milton Bache & Wickham, 2022), basemap (Schwalb-Willmann, 2024), dplyr (Wickham et al., 2023) and cowplot (Wilke, 2024). Distribution plots were constructed for DD, VB count and corrected ages. Scatterplots were constructed for size, band count and corrected age. The Single Logistic, Gompertz- and specialized von Bertalanffy growth functions, as given by Brey (2008), were applied to DD and corrected age data. The model parameters are given in Table 1, for which starting values were required.

Table 1. Names, equations and parameters of the growth functions applied to DD and corrected age data.

Function name	Equation	S_t	S_∞	t_o	t^*	K
Specialized van Bertalanffy	$S_t = S_\infty(1 - e^{-K^{-K(t-t_0)}})$	Size in cm DD at age t	Asymptotic size in cm DD	Age in years at which size S is zero		Growth constant per year
Gompertz	$S_t = S_\infty \times e^{-e^{-K(t-t^*)}}$				Age in years at the inflection point of the curve	
Single Logistic	$S_t = S_\infty \div (1 + e^{-K(t-t^*)}$					

The starting values were obtained by calculating a linear equation ($y = a + bx$) for the DD and corrected age data. The value for *b* was used as starting value for parameter *K*, while starting value for t_0 was obtained by solving the linear equation for when *y* was 0. The output from each growth model was used to plot the corresponding growth curve, and *RSS* and R^2 values were calculated to compare goodness-of-fit.

4 Results

4.1 Visualization of age bands

The alternating dark and light streaks giving rise to the pattern of growth bands (Fig. 10) were caused by changes in stereom density and elevated ridges (Fig. 10) on the fossa surface.

Figure 10. Changes in stereom density causing a pattern on the right upper fossa, yellow lines marking some of the visible growth bands.

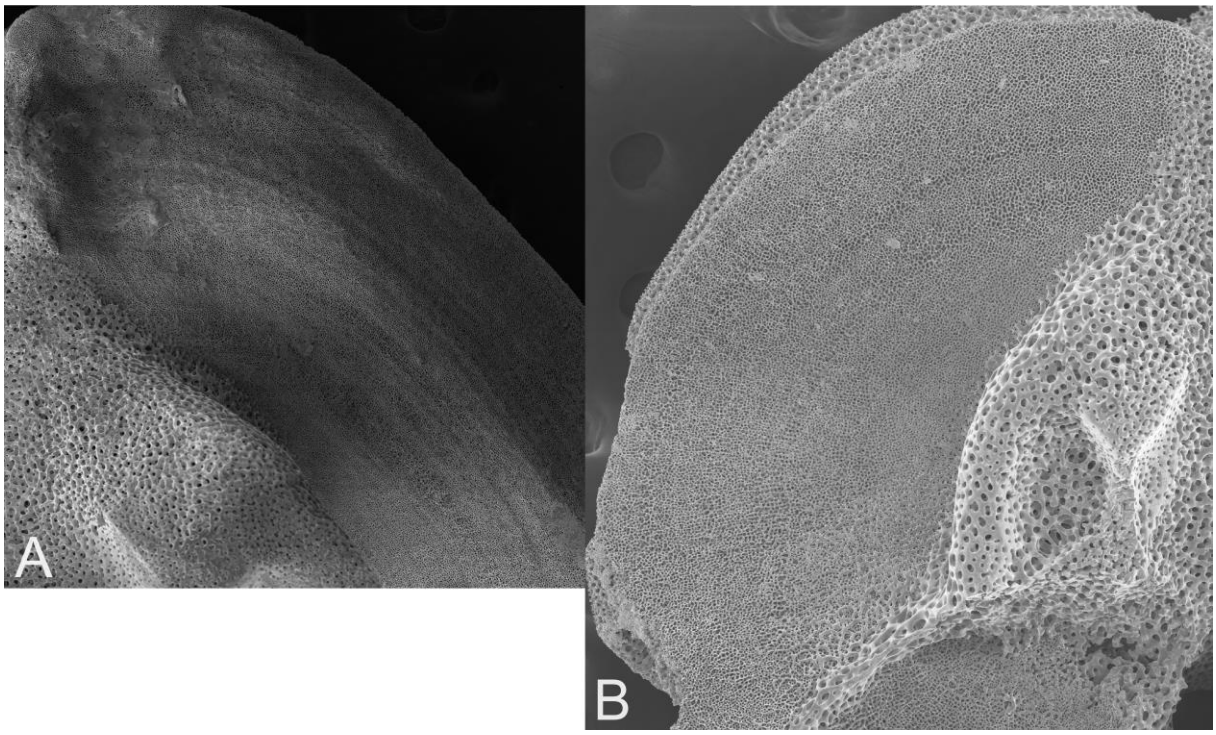

Figure 11. Collage showing ossicle fossa details of A) elevated ridges and B) changes in stereom density.

Except for a few ossicles with abnormal-looking stereom growth (probably due to previous injuries or malformation), growth bands were observed in all the examined ossicles regardless of which side was photographed. While band width was not measured, it was clear that it varied within a given ossicle.

Areas with denser stereom were generally brighter than those less dense, while ridges were brighter on the side facing the electron beam (Fig. 11). Areas with ridges and density changes often coincided, however this was hard to confirm due to the ossicles being photographed from only one angle: a difference in stereom density might not be discernable if the denser area is at a higher elevation (i.e. closer to the lens) caused by a ridge.

Two adjacent streaks of light and dark constituted one growth band, allowing individual bands to be marked and numbered on the right and left upper fossae in ImageJ (Fig. 12). Prior to numbering, the bands were inspected to ensure that a ridge and/or a density change was present.

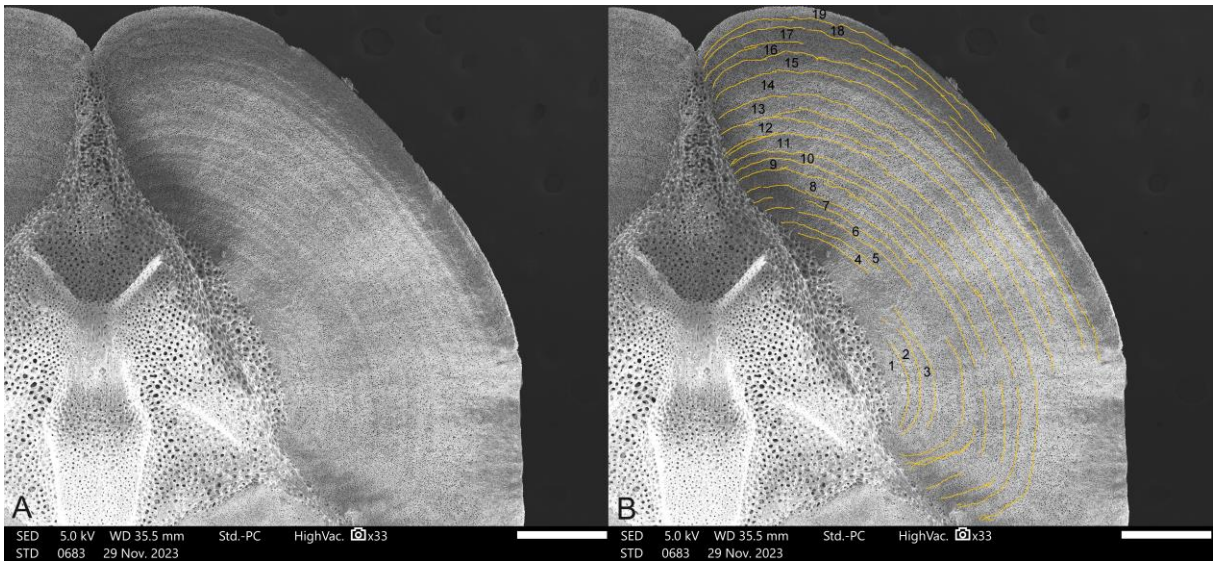

Figure 12. SEM-image showing A) the upper right fossa and B) the same image after marking and numbering visible growth bands.

In some instances, the articulation on the proximal side of ossicles had been damaged in a way such that the fossa surface was visible underneath (Fig. 13). This revealed faintly discernable continuation of growth bands.

Figure 13. Collage of three ossicles where a part of the articulating stereom had been damaged to reveal the fossa surface underneath. Yellow outlines marks where the articulation edge were believed to have been originally.

4.2 Age correction baseline

The established baseline for overgrown growth bands could correct for between 1-20 hidden bands, within a 0.59-2.28 mm distance from MP to VB1. The full baseline is presented below (Table 2) and was constructed using the MP-VB distances in 12 individuals.

Table 2. The baseline measurements used to determine how many growth bands were likely overgrown and had to be added the total band count of an individual. The mean MP-VB1 measurement in a given individual would fall into an interval given in the baseline, and the corresponding number of estimated hidden bands were added to the number of visible bands. In this way, a total band count was achieved and inferred to reflect age in years.

Interval in mm	N.o. hidden bands
< 0.59	0
0.59 ≤≥ 0.64	1
0.64 < > 0.72	2
0.72 ≤≥ 0.78	3
0.78 < > 0.83	4
0.83 ≤≥ 0.88	5
0.88 < > 1.04	6
1.04 ≤≥ 1.15	7
1.15 < > 1.26	8
1.26 ≤≥ 1.35	9
1.35 < > 1.40	10
1.40 ≤≥ 1.47	11
1.47 < > 1.54	12
1.54 ≤≥ 1.56	13
1.56 < > 1.72	14
1.72 ≤≥ 1.78	15
1.78 < > 1.92	16
1.92 ≤≥ 2.03	17
2.03 < > 2.14	18
2.14 ≤≥ 2.21	19
2.21 < > 2.28	20

4.3 Size, weight and band count distribution

In the 177 individuals from the original Barents Sea and Greenland samples, DDs ranged from 0.75 cm to 4.26 cm, with an overall mean of 2.50 cm. Close to a third of all individuals had a DD between 2.75-3.50 cm, while those measuring over 4 cm or under 1.50 cm were sparse among the Barents Sea individuals.

In the 80 individuals used for age analysis, the mean DD was 2.40 cm. The most common DD in the analyzed individuals was between 2.75-3.25 cm, with 33% of the analyzed individuals having a DD between 2.75-3.50 cm.

The distribution of DD measurements in all individuals and those analyzed both appear bimodal, with 2.75-3.50 cm DD constituting the largest mode. The smaller mode is visible in both distributions for DD measurements below 1.75 cm (Fig. 14).

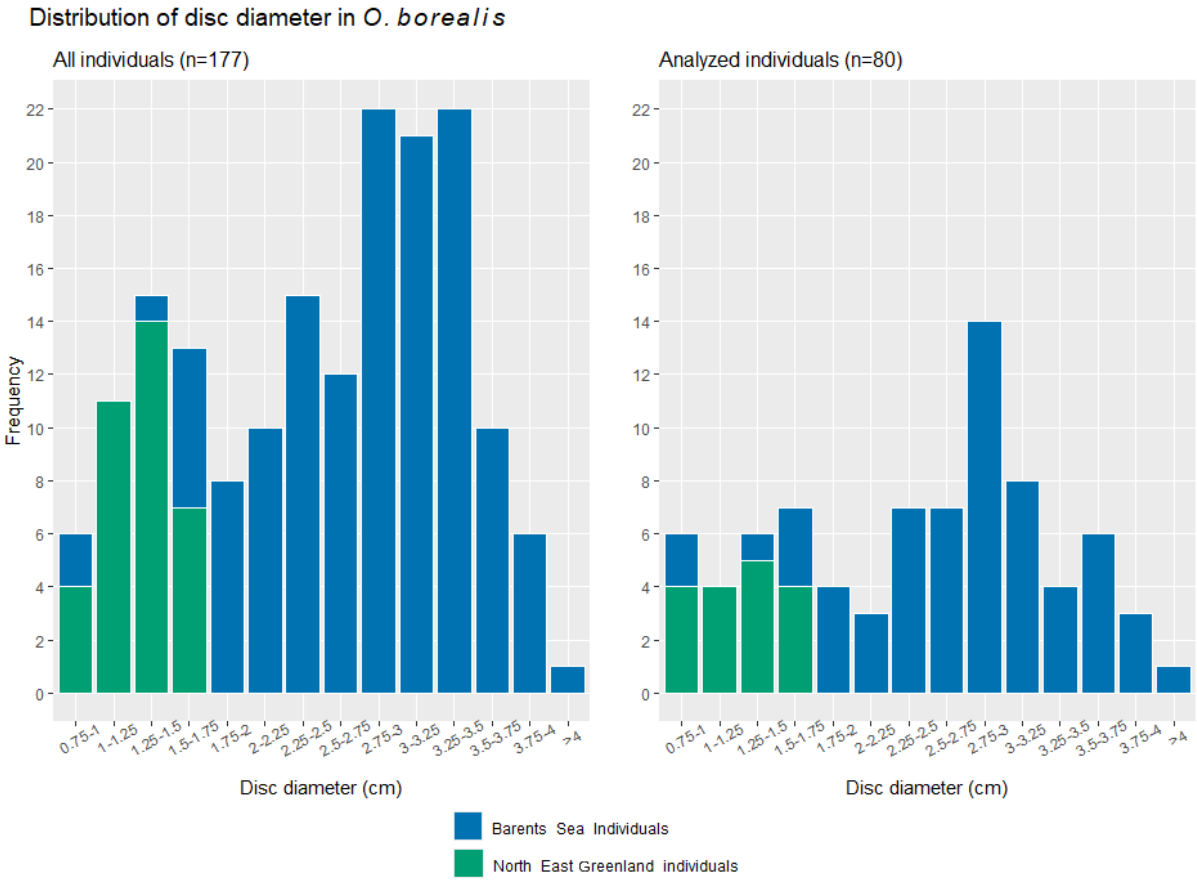

Figure 14. Histograms showing the distribution of mean disc diameter in all individuals of Ophiopleura borealis *measured, and in the individuals from which ossicles were used in age analysis.*

The blotted wet weight of the discs in 169 out of the 177 individuals ranged from 0.05-6.2 g, with a mean weight of 1.98 g. Disc weights were not obtained from the first eight individuals processed, although seven of them were still included in the age analysis. Out of the 80 analyzed individuals, blotted wet weight were obtained for 73. The weight range was between 0.05-6.2 g, with a mean disc weight of 1.87 g. The plotted distribution of disc weights (Fig. 15) show that in both all individuals and those analyzed, weights at the lower end of the x-axis was more common, with only one individual having the maximum weight.

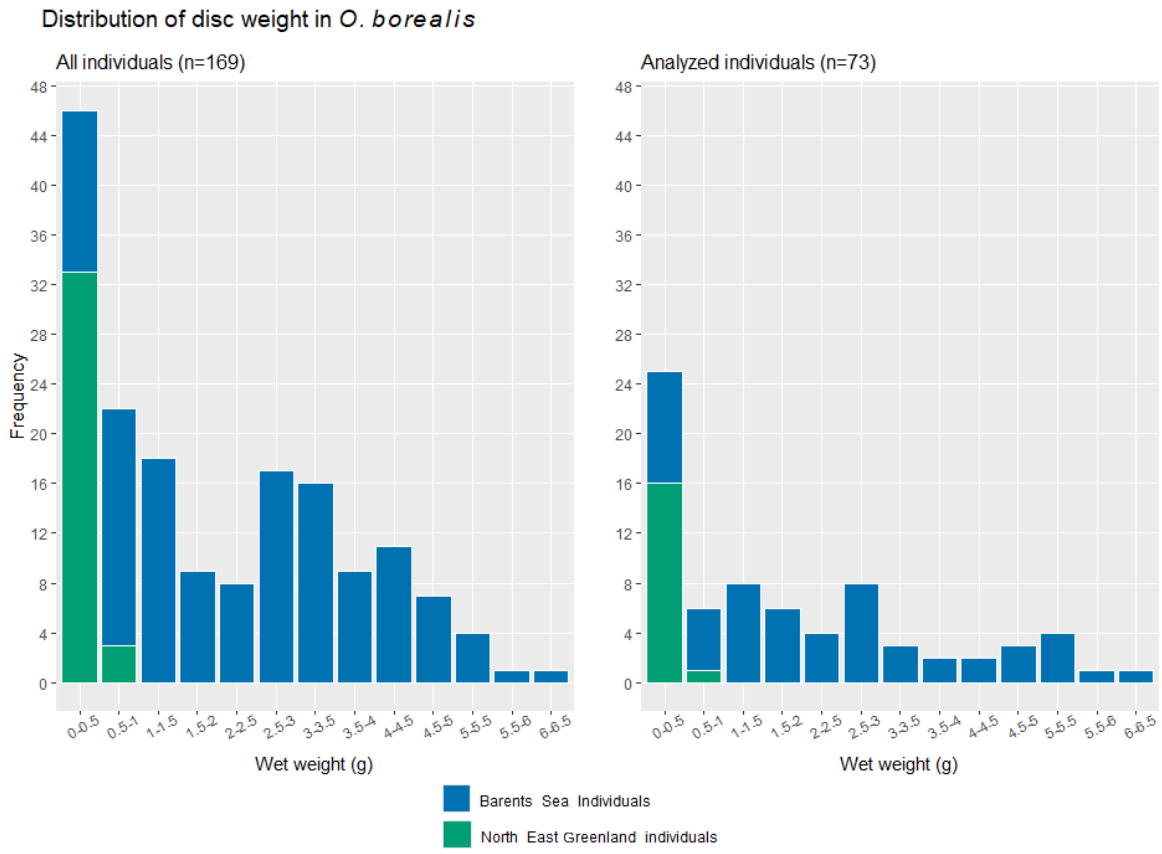

Figure 15. Histograms showing the distribution of disc weight in all individuals of Ophiopleura borealis measured, and in the individuals used for age analyis.

The number of visible growth bands ranged from 1 to 23, with a mean band count of 11. After age correction, brittle stars ranged from 1 to 39 years of age. The mean was 21 years. The distribution of growth band count (Fig. 16) show two modes: almost 20% of the individuals are in the first mode, defined by having 1-4 bands, and half of the individuals make up the second, larger, mode with 9-16 bands. In the histogram of corrected ages (Fig. 16) the distribution appear to have three modes. The first, smallest, mode is constituted by 3-8 year old individuals, followed by the second mode of 13-22 year olds which is about a third of the individuals. 40% of the individuals are in the largest and third mode, with ages between 25-32 years.

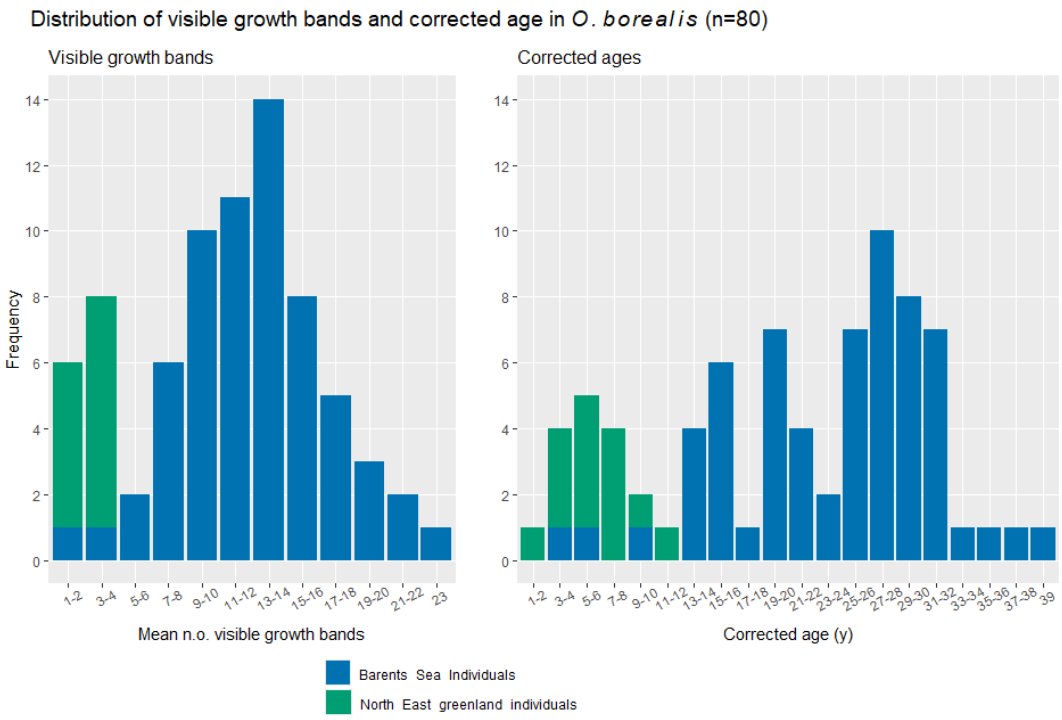

Figure 16. Histograms showing the distribution of mean number of visible growth bands per individual Ophiopleura borealis, and the age distribution following age correction.

The relationship between DD and the number of growth bands and ages were shown to be near-linear in scatterplots (Fig. 17), as the band count and age increase along with body size.

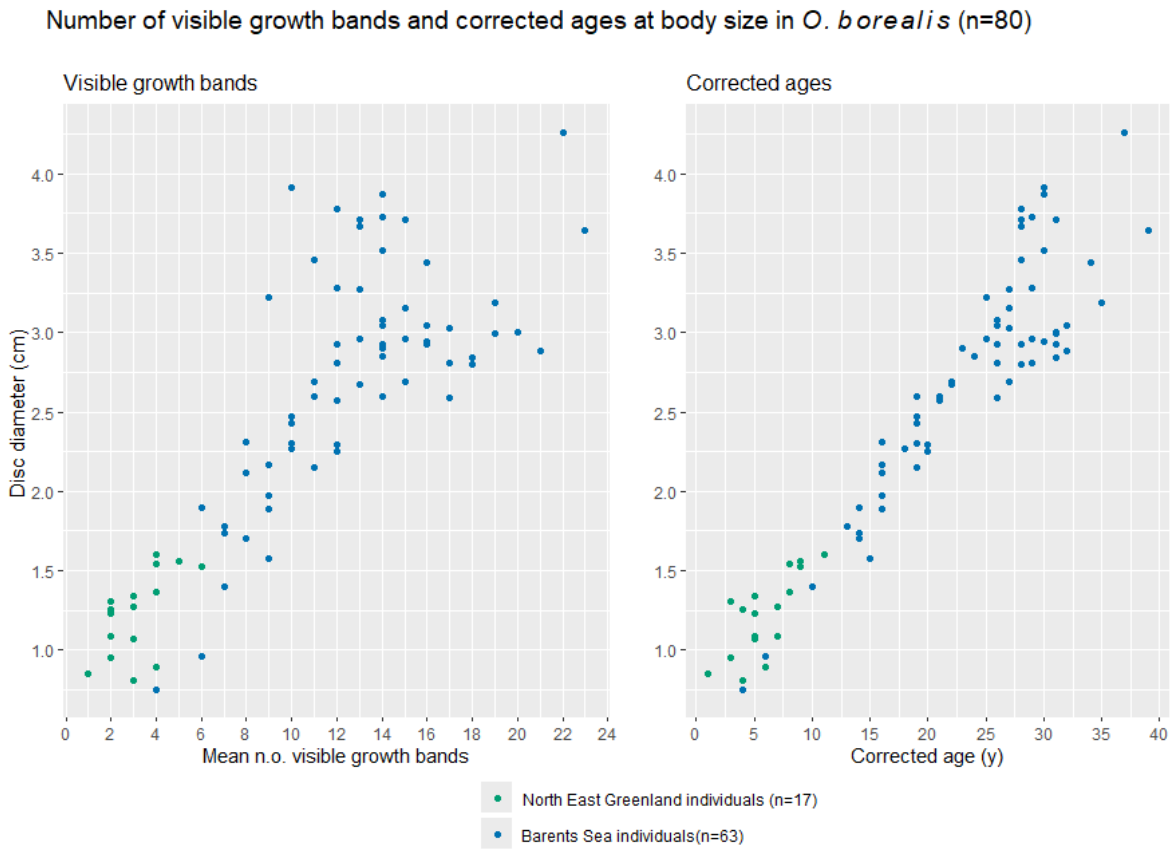

Figure 17. Scatterplots of the disc diameter and mean band count as well as the corrected ages in indviduals.

.

The linear equation calculated for the age and DD data was $y = 0.613 + 0.0858x$, meaning that the line had a slope of 0.0858 and intercepted the y-axis when $y = 0.613$. When $y = 0$, x was calculated as -8.15.

4.4 Growth models

The starting values for the model parameters were obtained from the linear equation calculated for DD and age. Starting value for parameter *K* (the growth constant) and t_o (age when size is 0) were 0.0858 and -8.15 respectively. S_∞ (asymptotic size) was given as the largest DD measured which was 4.26 cm. The starting value for *t** (age at inflection point) was 14 in the Gompertz model and 10 in the Single Logistic model. These were the same values the same as Ravelo et al. (2017) reported for *Ophiura sarsii* and *Ophiocten sericeum*, respectively, using the Gompertz model. The starting values are given in Table 3, together with the parameter output by each model and the corresponding *RSS* and R^2 values.

Table 3. Starting values used the first time running the models, and the values output from the models used for fitting and plotting the growth curves. RSS *and* R^2 *are also given for each function. Standard errors are given in parentheses.*

Parameter	K	t_o	t^*	S_∞	R^2	RSS
Starting values	0.0858	-8.15	14	4.26		
Specialized von Bertalanffy	0.01 (0.009)	-5.54 (2.06)		10.80 (7.30)	0.90	6.41
Gompertz	-0.05 (0.01)		12.96 (2.72)	4.92 (0.63)	0.90	6.21
Single Logistic	0.09 (0.011)		15.89 (1.84)	4.14 (0.30)	0.90	6.09

The asymptotic size estimated by the Specialized von Bertalanffy function was more than twice those given by the Gompertz and Single Logistic function, however it also had a markedly larger standard error. The Gompertz function estimated the lowest growth constant which also had the lowest standard error compared to the other growth constants. The age at the inflection point of the curve is estimated to be around 13 and 16 years according to the Gompertz and Single Logistic models respectively. All functions had an R^2 value of 0.90, while *RSS* values were 6.41 for Specialized von Bertalanffy, 6.21 for Gompertz and 6.09 for the Single Logistic.

The growth curves, constructed using the estimated parameters by corresponding function, are presented in Fig 18.

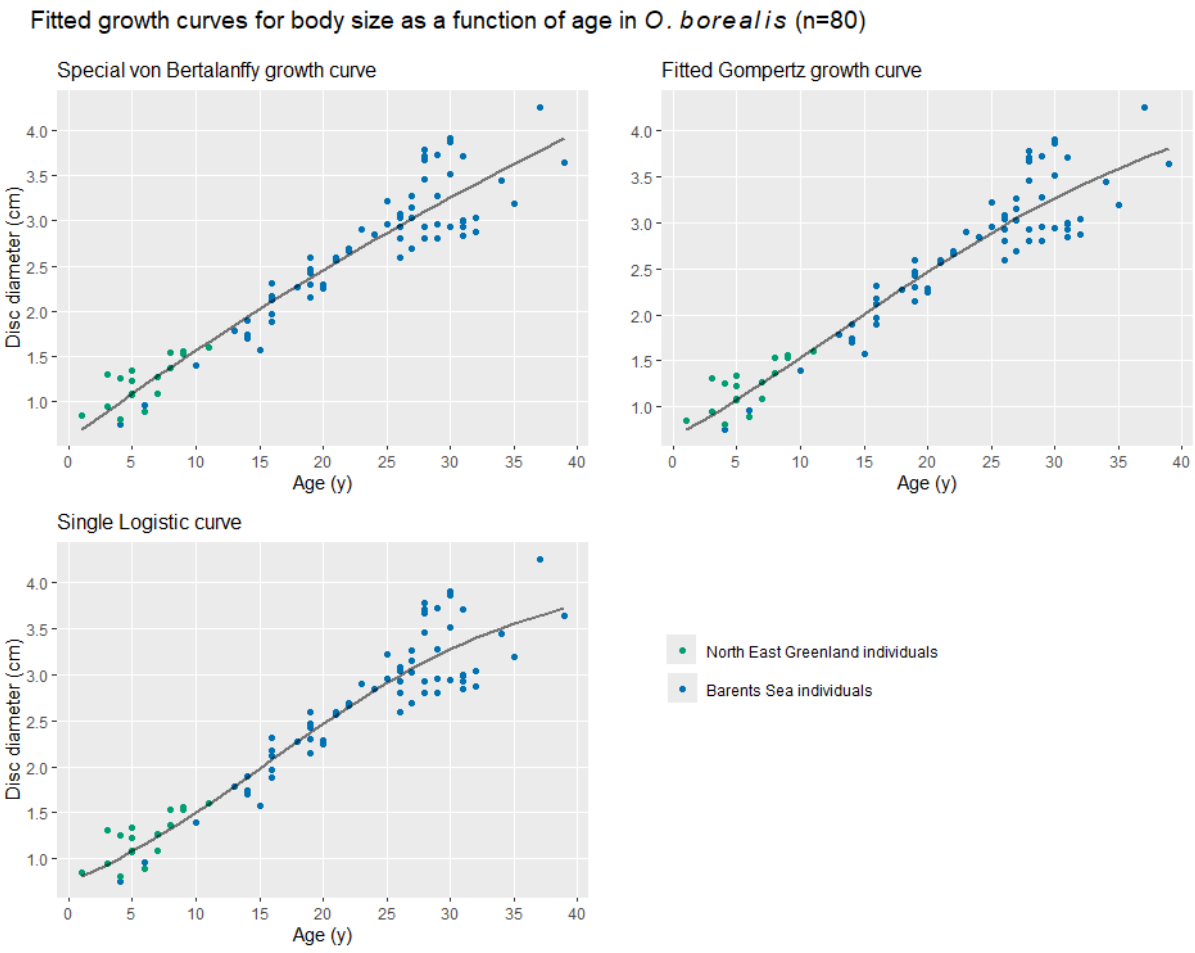

Figure 18. Fitted growth curves for the Specialized von Bertalanffy, Gompertz and Single Logistic functions, using the corresponding parameter outputs in Table 3.

5 Discussion

Growth bands were present in the ossicles of *Ophiopleura borealis* from both the Barents Sea and the Nort East Greenland samples, and were consistent with growth bands described in other brittle stars. This is in accordance with the first hypothesis:

1) Growth bands similar to those described in previous studies will be visible on the vertebrae ossicle surfaces.

Comparison of the disc diameter to the mean number of visible growth bands in individuals, a concurrent increase in both measurements was apparent (Fig. 17). This clearly indicate that larger, and thus older, individuals have more growth bands than smaller individuals. This relation could still be seen after age correction (Fig. 17). In both cases, however, there was a higher variability in the ages of individuals with a disc diameter over 2.5 cm. I believe this is due to the growth bands becoming thinner closer to the fossae edges, and harder to discern from each other in older individuals, which was evident during the analyses of SEM-images. This apparent decrease in width of the outer bands could reflect a decrease in growth rate as the brittle star grows older.

A maximum age of 39 years was inferred for *O. borealis*, and three growth models constructed, thus fulfilling the two main objectives of this study. In the following sections (5.1 and 5.2), I will discuss the second and third hypotheses:

2) *O. borealis* exhibits slower growth compared to brittle star species from lower latitudes.

3) The maximum age of the *O. borealis* specimens will exceed known ages for brittle stars from lower latitudes.

5.1 Longevity estimates in *Ophiopleura borealis,* other polar, temperate and subtropical brittle stars

Longevity estimates vary among brittle star species (Table 4). When comparing the maximum ages, it should be noted that the methods applied vary (Gorzula, 1977; Medeiros-Bergen & Ebert, 1995). They can differ in which skeletal parts have been analyzed for ageing, which growth functions have been used, or whether age correction have been applied. Yet, the subsequent comparison suggests a relationship with the climatic zones of geographic distribution. As no reported ages were found for brittle stars in the tropic, the studies in Table 4 only give the highest age estimates for a given species sampled within the Arctic, temperate, subtropical, or Antarctic regions.

The maximum age (39 years) of *O. borealis* exceed the estimates for all other studies presenting the highest maximum ages in brittle stars from the Arctic: *Ophiacanta bidentata* (15 years) (Stratanenko, 2021), *Stegophiura nodosa* (10 years) (Stratanenko & Denisenko, 2020), and *Ophiocten sericeum* (20 years) (Ravelo et al., 2017), and *Ophiura sarsii* (27 years) (Ravelo et al., 2017). Moreover, it is almost twice the maximum age estimates reported in brittle stars from temperate regions, which is 20 years in *Amphiura filiformis* and *Ophiomusa lymani* (*Ophiomusium lymani* in article) sampled from the west coast of Scotland and Ireland respectively (Gage, 1990; O'Connor et al., 1983). The highest estimates made for subtropical brittle stars belong to *Ophionereis annulata* and *Ophioplocus esmarki*. However, this study only estimated the age at which the two species are believed to reach 50% of their largest size, which is between nine to 11 years old (Medeiros-Bergen & Ebert, 1995). It is unlikely that the two species would be older than *O. borealis* at their largest size, as it takes around 20 years for *O. borealis* to reach half of its maximum size (Figs. 17, 18) which point to a slower growth rate than that of *Ophionereis annulata* and *Ophioplocus esmarki*. Only brittle star estimates from the Antarctic exceed the maximum age of *O. borealis*: Dahm (1996, referenced in Quiroga & Sellanes, 2009) reported maximum ages in four brittle star species from the Antarctic Weddell Sea: 19, 22, 25 and 33 years in *Ophioplocus incipiens (Ophioceres incipiens* in article), *Ophionotus victoriae, Ophioplinthus brevirima (Ophiurolepis brevirima* in article*)* and *Ophioplinthus gelida* (*Ophiurolepis gelida* in article), respectively.

In accordance with the third hypothesis, the maximum age estimates found in brittle stars from temperate regions were all lower than that for *O. borealis.*

Regarding the non-existent age estimates in brittle stars from the tropics, the lack of seasonality in the region makes it unlikely that the brittle stars would show any pronounced growth marks. However, sampling in tropical regions would be needed to confirm this.

Table 4. Summary of the maximum ages observed or estimated for brittle star species in different climatic zones (Arctic in blue text, temperate in green, subtropical in yellow and Antarctic in black), including the growth constant from if any growth models were applied in the study.

Region	**Species**	**Age (years)**	**Growth constant$_{model}$**	**Source**
Barents Sea and North East Greenland	*Ophiopleura borealis*	39 years	$0.01_{\text{Specialized von Bertalanffy}}$ -0.05_{Gompertz} $0.09_{\text{Single Logistic}}$	This study.
Chukchi sea	*Ophiura sarsii*	27 years	0.077_{Gompertz} $0.030_{\text{Specialized von Bertalanffy}}$	(Ravelo et al., 2017)
Beaufort Sea	*Ophiocten sericeum*	20 years	0.085_{Gompertz} $0.065_{\text{Specialized von Bertalanffy}}$	(Ravelo et al., 2017)
Vilkitsky strait, Severnaya Zemlya	*Ophiacantha bidentata*	10-15 years	$0.03_{\text{von Bertalanffy}}$	(Stratanenko, 2021)
Pechora Sea	*Stegophiura nodosa*	9-10 years	$0.09_{\text{von Bertalanffy}}$	(Stratanenko & Denisenko, 2020)
Chilean Sea	*Stegophiura* sp.	15 years	$0.078_{\text{von Bertalanffy}}$ $0.095_{\text{von Bertalanffy}}$ (near a cold-seep)	(Quiroga & Sellanes, 2009)
Firth of Lorne, South East of Scotland	*Ophiothrix fragilis*	9 years	$0.179_{\text{von Bertalanffy}}$	(Gage, 1990a)
West Coast of Ireland	*Amphiura filiformis*	≥20 years	NA	(O'Connor et al., 1983)

West Coast of Ireland	*Amphiura chiajei*	≥10 years	NA	(Munday & Keegan, 1992)
German Bight	*Ophiura ophiura*	9 years	$0.084_{\text{von Bertalanffy}}$	(Dahm, 1993)
German Bight	*Ophiura albida*	9 years	$0.229_{\text{von Bertalanffy}}$	(Dahm, 1993)
Funka Bay, South East of Hokkaido	*Ophiura sarsii* (*Ophiura sarsii sarsii* in article)	17 years	0.23_{Gompertz} $0.13_{\text{von Bertalanffy}}$ 0.32_{Logistic} 0.067_{Richard}	(Orino et al., 2019)
North West of Scotland and South West of Ireland	*Ophiocten hastatum*	10 years	0.20_{Gompertz} 0.63_{Richard}	(Gage et al., 2004)
Rockall Trough, North West of Scotland	*Ophiocten gracilis*	7 years	0.26_{Gompertz} $0.06_{\text{von Bertalanffy}}$	(Gage, 2003)
Rockall Trough, North West of Scotland	*Ophiura ljungmani*	10 years	0.51_{Gompertz} $0.27_{\text{van Bertalanffy}}$	(Gage, 1990a)
Rockall Trough, North West of Scotland	*Ophiomusa lymani* (*Ophiomusium lymani* in article)	20 years	0.56_{Gompertz} $0.36_{\text{von Bertalanffy}}$	(Gage, 1990a)
South West Coast of New Zealand	*Astrobrachion constrictum*	8 years	NA	(Stewart & Mladenov, 1997)
Firth of Clyde, West Coast of Scotland	*Ophiocomina nigra*	12-14 years	NA	(Gorzula, 1977)
South East Coast of Brazil	*Ophionereis reticulata*	6 years	$0.07_{\text{von Bertalanffy, seasonally oscillating}}$	(Yokoyama & Amaral, 2011)

False Point, San Diego Coast	*Ophionereis annulata*	>9-11 years	$0.075_{\text{Brody-Bertalanffy}}$	(Medeiros-Bergen & Ebert, 1995)
False Point, San Diego Coast	*Ophioplocus esmarki*	>9-11 years	$0.069_{\text{Brody-Bertalanffy}}$	(Medeiros-Bergen & Ebert, 1995)
Weddell Sea	*Ophionotus victoriae*	22 years	0.12_{Richard} 0.25_{Richard}	(Dahm, 1996)
Weddell Sea	*Ophioplinthus gelida* (*Ophiurolepis gelida* in article)	33 years	$0.041_{\text{von Bertalanffy}}$	(Dahm, 1996)
Weddell Sea	*Ophioplinthus brevirima* (*Ophiurolepis brevirima* in article)	25 years	$0.03_{\text{von Bertalanffy}}$	(Dahm, 1996)
Weddell Sea	*Ophioplocus incipiens* (*Ophioceres incipiens* in article)	19 years	$0.007_{\text{von Bertalanffy}}$	(Dahm, 1996)

5.2 Growth in *O. borealis*

Research on age and growth of commercially valuable fish and marine invertebrates have long been conducted in the fishing industry, as it provides information necessary for stock assessment and management (Campana & Thorrold, 2001; Helidoniotis et al., 2011). Some of the most commonly used growth models are the von Bertalanffy and the Gompertz models (Helidoniotis et al., 2011), albeit no model is universally applicable to all species (Hirst & Forster, 2013).

Ophiuroid growth curves are often sigmoid or logarithmic in shape (Dahm & Brey, 1998; Quiroga & Sellanes, 2009; Ravelo et al., 2017; Sköld et al., 2001), however, this was not the case in all curves constructed for *O. borealis* (Fig. 18). While the growth rate in brittle stars is generally expected to decrease as a maximum body size is approached (Ravelo et al., 2017), only the Single Logistic and the Gompertz (Fig. 18) growth curves indicated such a trajectory for *O. borealis.* In both curves, a slight decrease in growth rate can be seen at the further end of the x-axis, but neither one reaches the asymptotic size estimated by the corresponding growth function. The R^2 values were very high, and were the same for all three functions, while *RSS* values varied. The lowest value was that of the Single Logistic function, while the Specialized von Bertalanffy function yielded the highest *RSS* value. This indicates that the Specialized von Bertalanffy model was the least fitting of the applied models in this study. The considerably large asymptotic size estimated by the Specialized von Bertalanffy function could also indicate that it was not the most suitable one, while the estimates by the Gompertz and the Single Logistic functions were more similar to each other and had lower standard errors as well. While few brittle star species exceed a disc diameter of five cm, a disc size larger than 10 cm is not fully unrealistic in ophiuroids as the largest gorgonocephalid species can reach a disc diameter of 15 cm (Stöhr et al., 2012).

When addressing the second hypothesis regarding a slower growth in *O. borealis* compared to brittle stars from lower latitudes, it is difficult to arrive at a definitive answer. However, based on the growth constants in Table 4, albeit estimated by different growth functions, all studies on Arctic and Antarctic species presented growth constants lower than 0.1. In temperate regions, however, growth constants between 0.13 and 0.63 were more common. Some of the growth constants reported for temperate brittle stars are closer to those estimated in the polar species. Interestingly, this is also the case for the subtropical species, contradicting the second hypothesis. However, only two studies provided the growth constant estimates for the

subtropical brittle stars, and more studies would be needed in order to make a more solid comparison between the different regions. It should be noted that growth similarities between species or populations in different regions is not unexpected, as factors affecting growth vary across other aspects than only latitude. Differences in, for example, food availability and amount of disturbance can be connected to depth (Montero-Serra et al., 2018).

5.3 Limitations of the current study

A limitation of this study is the combination of individuals from two distinct populations. While this approach was deemed justifiable given the primary objective of deriving age estimates *O. borealis*, it must be acknowledged that the growth models may not accurately represent any of the populations sampled in this study.

It proved somewhat difficult to secure ossicles of good quality (i.e. free from tissue, debris or damage) for SEM analysis. It was rare for all ossicles from an individual to be of good quality, meaning that the number of visible growth bands were inconsistent between ossicles. Yet, this appear to be one of the few studies that made the effort to analyze several ossicles per individual and used the mean values from up to three ossicles per individual. In two individuals, the difference in the number of visible bands between the ossicle with the lowest and highest band count, were nine and 10.5 respectively - albeit I considered this difference to be rather extreme. It indicates, however, the possibility of high variabilities in the number of visible bands between the ossicles of a given individual.

Due to time constraints, no validation of the annual formation of growth bands observed in *O. borealis* could be performed in this study. Previous studies, however, have validated the annual periodicity of growth patterns in marine echinoderms (Brey et al., 1995; Gage, 1992; Sun et al., 2019), and indicated this to be the case in brittle stars as well (Dahm, 1993; Gorzula, 1977). Originally, such validation techniques were developed for fish otoliths. It is common to either keep individuals in culture or in situ for observation, by for example rearing juveniles in an aquarium to know their exact age or recapture previously marked individuals in a wild population (Stump & Lucas, 1990; Sun et al., 2019). The latter is known as mark-recapture, which often utilizes fluorescent dye that binds to the outer, growing parts of the organisms' carbonate structure (Gage, 1992). Upon recapture, the number or width of growth bands that have been produced in the time since marking an individual can be estimated. A

study on age determination in echinoderms from 2019 (Sun et al.) for example, utilized both techniques to successfully confirm that formation of growth bands in the cold-water sea cucumber *Psolus fabricii* were indeed annual.

While a number of species have undergone band validation, the assumption of un-validated growth bands forming annually is widespread. There are studies on other echinoderms refuting annual band formation (Hill et al., 2004; Narvaez et al., 2016; Russell & Meredith, 2000). In a study from 2016, Narvaez et al (2016) subjected sea urchins to different temperature- and feeding regimes, after which growth typically associated with warmer temperatures were observed in sea urchins subjected to cold temperature and vice versa. While this may contradict the notion of seasonal temperature differences driving growth band formation, the fact that the sea urchins were removed from their natural habitat and kept in artificial conditions should be taken into consideration. Meanwhile, the study by Sun et al. (2019) in which sea cucumbers were reared in captivity, did not see significantly different formation of growth patterns when compared to wild sea cucumbers.

6 Conclusions and future studies

This study has shown that growth bands are indeed present in the Arctic brittle star *Ophiopleura borealis*, and yielded the first ever age estimates for the species. Although the estimated growth constants for *O. borealis* were similar to those estimated for other polar brittle stars, a handful of temperate and subtropical species had even lower growth constants. Thus, *O. borealis* cannot be said to exhibit slower growth than all brittle star species from lower latitudes. The maximum age, 39 years, for *O. borealis* did exceed all maximum ages reported in brittle stars from lower latitudes. The combination of slow growth and high age, however, may indicate *O. borealis* as less resilient to disturbances. Apart from the need for more studies on longevity in brittle stars, particularly from different latitudes, future research would also benefit from validation of annual growth band formation when ageing brittle stars.

Works cited

Abdelhady, A. A., Seuss, B., Jain, S., Abdel-Raheem, K. H. M., Elsheikh, A., Ahmed, M. S., Elewa, A. M. T., & Hussain, A. M. (2024). New and emerging technologies in paleontology and paleobiology: A horizon scanning review. *Journal of African Earth Sciences*, *210*, 105155. https://doi.org/10.1016/j.jafrearsci.2023.105155

Al-Habahbeh, A. K., Kortsch, S., Bluhm, B. A., Beuchel, F., Gulliksen, B., Ballantine, C., Cristini, D., & Primicerio, R. (2020). Arctic coastal benthos long-term responses to perturbations under climate warming. *Philosophical Transactions of the Royal Society A: Mathematical, Physical and Engineering Sciences*, *378*(2181), 20190355. https://doi.org/10.1098/rsta.2019.0355

Andrus, C. F. T., Bassett, C. N., Voorhies, B., & Moyes, H. (2024). Ritual schedule and worshippers' origin at an ancient Maya ritual cave site, Las Cuevas, Belize: A pilot study of *jute* snail shell sclerochemistry. *Journal of Archaeological Science: Reports*, *53*, 104371. https://doi.org/10.1016/j.jasrep.2023.104371

Aphalo, P. J. (2023). *ggpmisc: Miscellaneous Extensions to 'ggplot2'* ({R package version 0.5.5) [Computer software]. https://CRAN.R-project.org/package=ggpmisc

Arctic PRIZE — Scottish Association for Marine Science, Oban UK. Retrieved 18 April 2024, from https://www.sams.ac.uk/science/projects/arctic-prize/#:~:text=The%20Arctic%20PRIZE%20project%20addresses,structure%20of%20the%20Arctic%20Ocean.

Bluhm, B. A., Piepenburg, D., & von Juterzenka, K. (1998). Distribution, standing stock, growth, mortality and production of *Strongylocentrotus pallidus* (Echinodermata: Echinoidea) in the northern Barents Sea. *Polar Biology*, *20*(5), 325–334. https://doi.org/10.1007/s003000050310

Brey, T., Pearse, J., Basch, L., McClintock, J., & Slattery, M. (1995). Growth and production of *Sterechinus neumayeri* (Echinoidea: Echinodermata) in McMurdo Sound, Antarctica. *Marine Biology*, *124*(2), 279–292. https://doi.org/10.1007/BF00347132

Broom, D. M. (1975). Aggregation behaviour of the brittle-star *Ophiothrix fragilis*. *Journal of the Marine Biological Association of the United Kingdom*, *55*(1), 191–197. Scopus. https://doi.org/10.1017/S0025315400015836

Buddemeier, R. W., Maragos, J. E., & Knutson, D. W. (1974). Radiographic studies of reef coral exoskeletons: Rates and patterns of coral growth. *Journal of Experimental Marine Biology and Ecology*, *14*(2), 179–199. https://doi.org/10.1016/0022-0981(74)90024-0

Burukovsky, R. N., Syomin, V. L., Zalota, A. K., Simakov, M. I., & Spiridonov, V. A. (2021). Food Spectra of Snow Crabs (*Chionoecetes opilio* (O. Fabricius, 1788) (Decapoda, Oregoniidae), Non-Indigenous Species of the Kara Sea. *Oceanology*, *61*(6), 964–975. https://doi.org/10.1134/S0001437021060205

Calero, B., Ramos, A., & Ramil, F. (2018). An uncommon or just an ecologically demanding species? Finding of aggregations of the brittle-star *Ophiothrix maculata* on the Northwest African slope. *Deep Sea Research Part I: Oceanographic Research Papers*, *131*, 87–92. https://doi.org/10.1016/j.dsr.2017.11.008

Campana, S., & Thorrold, S. (2001). Otoliths, increments, and elements: Keys to a comprehensive understanding of fish populations? *Canadian Journal of Fisheries and Aquatic Sciences - CAN J FISHERIES AQUAT SCI*, *58*, 30–38. https://doi.org/10.1139/cjfas-58-1-30

Dahm, C. (1993). Growth, production and ecological significance of *Ophiura albida* and *O. ophiura* (Echinodermata: Ophiuroidea) in the German Bight. *Marine Biology*, *116*(3), 431–437. https://doi.org/10.1007/BF00350060

Dahm, C. (1996). *Ökologie und Populationsdynamik antarktischer Ophiuroiden (Echinodermata) = Ecology and population dynamcis of Antarctic ophiuroids (Echinodermata)* ['Berichte zur Polar- und Meeresforschung' (PhD), Alfred Wegener Institute for Polar and Marine Research]. https://epic.awi.de/id/eprint/26372/

Dahm, C., & Brey, T. (1998). Determination of Growth and Age of Slow Growing Brittle Stars (Echinodermata: Ophiuroidea) From Natural Growth Bands. *Journal of the Marine Biological Association of the United Kingdom*, *78*(3), 941–951. https://doi.org/10.1017/S0025315400044891

Dauvin, J.-C., Méar, Y., Murat, A., Poizot, E., Lozach, S., & Beryouni, K. (2013). Interactions between aggregations and environmental factors explain spatio-temporal patterns of the brittle-star *Ophiothrix fragilis* in the eastern Bay of Seine. *Estuarine, Coastal and Shelf Science*, *131*, 171–181. https://doi.org/10.1016/j.ecss.2013.07.005

Davoult, D., & Migné, A. (2001). Respiration and excretion of a dense *Ophiothrix fragilis* population in the Bay of Seine (English Channel, France). In *Echinoderm 2000* (pp. 243–248).

Drolet, D., Himmelman, J. H., & Rochette, R. (2004). Use of refuges by the ophiuroid *Ophiopholis aculeata*: Contrasting effects of substratum complexity on predation risk from two predators. *Marine Ecology Progress Series*, *284*, 173–183.

Elzhov, T., Mullen, K., Spiess, A., & Bolker, B. (2023). *minpack.lm: R Interface to the Levenberg-Marquardt Nonlinear Least-Squares Algorithm Found in MINPACK, Plus Support for Bounds.* (R package version 1.2-4) [Computer software]. CRAN.R-project.org/package=minpack.lm

Frainer, A., Primicerio, R., Kortsch, S., Aune, M., Dolgov, A. V., Fossheim, M., & Aschan, M. M. (2017). Climate-driven changes in functional biogeography of Arctic marine

fish communities. *Proceedings of the National Academy of Sciences of the United States of America*, *114*(46), 12202–12207. https://doi.org/10.1073/pnas.1706080114

Freire, J., & González-Gurriarán, E. (1995). Feeding ecology of the velvet swimming crab *Necora puber* in mussel raft areas of the Ría de Arousa (Galicia, NW Spain). *Marine Ecology Progress Series*, *119*(1/3), 139–154.

Fujita, T., & Ohta, S. (1989). Spatial structure within a dense bed of the brittle star *Ophiura sarsi* (Ophiuroidea: Echinodermata) in the bathyal zone off otsuchi, Northeastern Japan. *Journal of Oceanography*, *45*(5), 289–300. https://doi.org/10.1007/BF02123483

Gage, J. D. (1990a). Skeletal growth bands in brittle stars: Microstructure and significance as age markers. *Journal of the Marine Biological Association of the United Kingdom*, *70*(1), 209–224. https://doi.org/10.1017/S0025315400034329

Gage, J. D. (1990b). Skeletal growth markers in the deep-sea brittle stars *Ophiura ljungmani* and *Ophiomusium lymani*. *Marine Biology*, *104*(3), 427–435. https://doi.org/10.1007/BF01314346

Gage, J. D. (1992). Natural growth bands and growth variability in the sea urchin *Echinus esculentus*: Results from tetracycline tagging. *Marine Biology*, *114*(4), 607–616. https://doi.org/10.1007/BF00357257

Gage, J. D. (2003). Growth and production of *Ophiocten gracilis* (Ophiuroidea: Echinodermata) on the Scottish continental slope. *Marine Biology*, *143*(1), 85–97. https://doi.org/10.1007/s00227-003-1050-7

Gage, J. D., Anderson, R. M., Tyler, P. A., Chapman, R., & Dolan, E. (2004). Growth, reproduction and possible recruitment variability in the abyssal brittle star *Ophiocten hastatum* (Ophiuroidea: Echinodermata) in the NE Atlantic. *Deep-Sea Research. Part*

I, Oceanographic Research Papers, *51*(6), 849–864. https://doi.org/10.1016/j.dsr.2004.01.007

Gallagher, M. L., Ambrose, W. G., & Renaud, P. E. (1998). Comparative studies in biochemical composition of benthic invertebrates (bivalves, ophiuroids) from the Northeast Water (NEW) Polynya. *Polar Biology*, *19*(3), 167–171. https://doi.org/10.1007/s003000050230

Gaymer, C. F., Dutil, C., & Himmelman, J. H. (2004). Prey selection and predatory impact of four major sea stars on a soft bottom subtidal community. *Journal of Experimental Marine Biology and Ecology*, *313*(2), 353–374. https://doi.org/10.1016/j.jembe.2004.08.022

Geraldi, N., Bertolini, C., Emmerson, M., Roberts, D., & O'Connor, N. (2016). Aggregations of brittle stars can provide similar ecological roles as mussel reefs. *Marine Ecology Progress Series*, *563*. https://doi.org/10.3354/meps11993

Gorzula, S. (1977). A study of growth in the brittle-star *Ophiocomina nigra*. *Western Naturalist, 6: 13-33.* https://www.academia.edu/42962835/A_study_of_growth_in_the_brittle_star_Ophiocomina_nigra

Grebmeier, J. M., Overland, J. E., Moore, S. E., Farley, E. V., Carmack, E. C., Cooper, L. W., Frey, K. E., Helle, J. H., McLaughlin, F. A., & McNutt, S. L. (2006). A Major Ecosystem Shift in the Northern Bering Sea. *Science*, *311*(5766), 1461–1464.

Helidoniotis, F., Haddon, M., Tuck, G., & Tarbath, D. (2011). The relative suitability of the von Bertalanffy, Gompertz and inverse logistic models for describing growth in blacklip abalone populations (*Haliotis rubra*) in Tasmania, Australia. *Fisheries Research*, *112*(1), 13–21. https://doi.org/10.1016/j.fishres.2011.08.005

Hill, S., Aragona, J., & Lawrence, J. (2004). Growth Bands in Test Plates of the Sea Urchins *Arbacia punctulata* and *Lytechinus variegatus* (Echinodermata) on the Central Florida Gulf Coast Shelf. *Gulf of Mexico Science*, *22*, 96–100. https://doi.org/10.18785/goms.2201.09

Hinz, H., Kröncke, I., & Ehrich, S. (2005). The feeding strategy of dab *Limanda limanda* in the southern North Sea: Linking stomach contents to prey availability in the environment. *Journal of Fish Biology*, *67*(sB), 125–145. https://doi.org/10.1111/j.0022-1112.2005.00918.x

Hirst, A. G., & Forster, J. (2013). When growth models are not universal: Evidence from marine invertebrates. *Proceedings: Biological Sciences*, *280*(1768), 1–7.

Hudson, J. H., Shinn, E. A., Halley, R. B., & Lidz, B. (1976). Sclerochronology: A tool for interpreting past environments. *Geology*, *4*(6), 361–364. https://doi.org/10.1130/0091-7613(1976)4<361:SATFIP>2.0.CO;2

Hüssy, K., Andersen, N. G., & Pedersen, E. M. (2016). The influence of feeding behaviour on growth of Atlantic cod (*Gadus morhua*, Linnaeus, 1758) in the North Sea. *Journal of Applied Ichthyology*, *32*(5), 928–937. https://doi.org/10.1111/jai.13160

Ingvaldsen, R., Bluhm, B., Aberle-Malzahn, N., Amundsen, R., Ardelan, M. V., Bagøien, E., Bratbak, G., Bratrein, M., Chierici, M., Descoteux, R., Dietrich, U., Divine, D., Ellingsen, P. G., Fransson, A., Halvorsen, E., Hoff, S., Holm, E., Jentoft, S., Jones, E., … Åström, E. (2020). Joint Cruise 1-2 2018: Cruise Report. *The Nansen Legacy Report Series*, *4*, Article 4. https://doi.org/10.7557/nlrs.5628

Intergovernmental Panel on Climate Change (IPCC) (Ed.). (2022). Polar Regions. In *The Ocean and Cryosphere in a Changing Climate: Special Report of the Intergovernmental Panel on Climate Change* (pp. 203–320). Cambridge University Press. https://doi.org/10.1017/9781009157964.005

Ivanova, S. V., Kessel, S. T., Espinoza, M., McLean, M. F., O'Neill, C., Landry, J., Hussey, N. E., Williams, R., Vagle, S., & Fisk, A. T. (2020). Shipping alters the movement and behavior of Arctic cod (*Boreogadus saida*), a keystone fish in Arctic marine ecosystems. *Ecological Applications*, *30*(3), e02050. https://doi.org/10.1002/eap.2050

Kassambara, A. (2023). *ggpubr: 'ggplot2' Based Publication Ready Plots* (R package version 0.6.0) [Computer software]. https://CRAN.R-project.org/package=ggpubr

Kortsch, S., Primicerio, R., Beuchel, F., Renaud, P. E., Rodrigues, J., Lønne, O. J., & Gulliksen, B. (2012). Climate-driven regime shifts in Arctic marine benthos. *Proceedings of the National Academy of Sciences*, *109*(35), 14052–14057. https://doi.org/10.1073/pnas.1207509109

Leeuwenhoek, A. V. (1685). An abstract of a letter of Mr. Anthony Leewenhoek Fellow of the R. Society; concerning the parts of the brain of severall animals; the chalk stones of the gout; the leprosy; and the scales of eeles. *Philosophical Transactions of the Royal Society of London*, *15*(168), 883–895. https://doi.org/10.1098/rstl.1685.0015

Medeiros-Bergen, D. E., & Ebert, T. A. (1995). Growth, fecundity and mortality rates of two intertidal brittlestars (Echinodermata: Ophiuroidea) with contrasting modes of development. *Journal of Experimental Marine Biology and Ecology*, *189*(1), 47–64. https://doi.org/10.1016/0022-0981(95)00010-O

Milton Bache, S., & Wickham, H. (2022). *magrittr: A Forward-Pipe Operator for R* (R package version 2.0.3) [Computer software]. https://CRAN.R-project.org/package=magrittr

Montero-Serra, I., Linares, C., Doak, D. F., Ledoux, J. B., & Garrabou, J. (2018). Strong linkages between depth, longevity and demographic stability across marine sessile species. *Proceedings of the Royal Society B: Biological Sciences*, *285*(1873). https://doi.org/10.1098/rspb.2017.2688

Morata, N., Michaud, E., Poullaouec, M.-A., Devesa, J., Le Goff, M., Corvaisier, R., & Renaud, P. E. (2020). Climate change and diminishing seasonality in Arctic benthic processes. *Philosophical Transactions of the Royal Society A: Mathematical, Physical and Engineering Sciences*, *378*(2181), 20190369. https://doi.org/10.1098/rsta.2019.0369

Munday, B. W., & Keegan, B. F. (1992). Population dynamics of *Amphiura chiajei* (Echinodermata: Ophiuroidea) in Killary Harbour, on the west coast of Ireland. *Marine Biology*, *114*(4), 595–605. https://doi.org/10.1007/BF00357256

Narvaez, C. A., Johnson, L. E., & Sainte-Marie, B. (2016). Growth bands are an unreliable indicator of sea urchin age: Evidence from the laboratory and the literature. *Limnology and Oceanography: Methods*, *14*(8), 527–541. https://doi.org/10.1002/lom3.10110

Neves, B. de M., Edinger, E., Layne, G. D., & Wareham, V. E. (2015). Decadal longevity and slow growth rates in the deep-water sea pen *Halipteris finmarchica* (Sars, 1851) (Octocorallia: Pennatulacea): implications for vulnerability and recovery from anthropogenic disturbance. *Hydrobiologia*, *759*(1), 147–170. https://doi.org/10.1007/s10750-015-2229-x

O'Connor, B., Bowmer, T., & Grehan, A. (1983). Long-term assessment of the population dynamics of *Amphiura filiformis* (Echinodermata: Ophiuroidea) in Galway Bay (west coast of Ireland). *Marine Biology*, *75*(2), 279–286. https://doi.org/10.1007/BF00406013

Orino, K., Ishigane, K., Suzuki, K., Izumiura, H., Nakaya, M., & Takatsu, T. (2019). Growth of the brittle star *Ophiura sarsii sarsii* in Funka Bay, Hokkaido, Japan. *Fisheries Science*, *85*(4), 705–716. https://doi.org/10.1007/s12562-019-01323-1

Oschmann, W. (2009). Sclerochronology: Editorial. *International Journal of Earth Sciences*, *98*(1), 1–2. https://doi.org/10.1007/s00531-008-0403-3

Peharda, M., Gillikin, D. P., Schöne, B. R., Verheyden, A., Uvanović, H., Markulin, K., Šarić, T., Janeković, I., & Župan, I. (2022). Nitrogen Isotope Sclerochronology—Insights Into Coastal Environmental Conditions and Pinna nobilis Ecology. *Frontiers in Marine Science*, *8*. https://doi.org/10.3389/fmars.2021.816879

Piepenburg, D. (2000). Arctic Brittle Stars (Echinodermata: Ophiuroidea). In *Oceanography and Marine Biology: An Annual Review: Volume 38*. CRC Press.

Piepenburg, D. (2005). Recent research on Arctic benthos: Common notions need to be revised. *Polar Biology*, *28*(10), 733–755. https://doi.org/10.1007/s00300-005-0013-5

Piepenburg, D., & Schmid, M. K. (1996). Brittle star fauna (Echinodermata: Ophiuroidea) of the arctic northwestern Barents sea: composition, abundance, biomass and spatial distribution. *Polar Biology*, *16*(6), 383–392. https://doi.org/10.1007/BF02390420

Piepenburg, D., & von Juterzenka, K. (1994). Abundance, biomass and spatial distribution pattern of brittle stars (Echinodermata: Ophiuroidea) on the Kolbeinsey Ridge north of Iceland. *Polar Biology*, *14*(3), 185–194. https://doi.org/10.1007/BF00240523

Piepenburg, D., Voß, J., & Gutt, J. (1997). Assemblages of sea stars (Echinodermata: Asteroidea) and brittle stars (Echinodermata: Ophiuroidea) in the Weddell Sea (Antarctica) and off Northeast Greenland (Arctic): a comparison of diversity and abundance. *Polar Biology*, *17*(4), 305–322. https://doi.org/10.1007/PL00013372

Pulteney, R. (1781). *A general view of the writings of Linnaeus*. Printed for T. Payne ...; and B. White. https://doi.org/10.5962/bhl.title.96885

Quiroga, E., & Sellanes, J. (2009). Growth and size-structure of *Stegophiura* sp. (Echinodermata: Ophiuroidea) on the continental slope off central Chile: a comparison between cold seep and non-seep sites. *Journal of the Marine Biological Association of the United Kingdom*, *89*(2), 421–428. https://doi.org/10.1017/S0025315408002786

R Core Team. (2023). *R: A Language and Environment for Statistical Computing* (4.3.2) [Computer software]. R Foundation for Statistical Computing. www.R-project.org

Ravelo, A. M., Konar, B., Bluhm, B., & Iken, K. (2017). Growth and production of the brittle stars *Ophiura sarsii* and *Ophiocten sericeum* (Echinodermata: Ophiuroidea). *Continental Shelf Research*, *139*, 9–20. https://doi.org/10.1016/j.csr.2017.03.011

Ravelo, A. M., Konar, B., Trefry, J. H., & Grebmeier, J. M. (2014). Epibenthic community variability in the northeastern Chukchi Sea. *Deep Sea Research Part II: Topical Studies in Oceanography*, *102*, 119–131. https://doi.org/10.1016/j.dsr2.2013.07.017

Roman Gonzalez, A. (2021). Sclerochronology in the Southern Ocean. *Polar Biology*, *44*(8), 1485–1515. https://doi.org/10.1007/s00300-021-02899-0

Rowe, S., & Smith, B. E. (2022). Food web ecology of Gulf Stream flounder (*Citharichthys arctifrons*): A continental shelf perspective. *Journal of Fish Biology*, *101*(5), 1199–1209. https://doi.org/10.1111/jfb.15190

Russell, M. P., & Meredith, R. W. (2000). Natural growth lines in echinoid ossicles are not reliable indicators of age: A test using *Strongylocentrotus droebachiensis*. *Invertebrate Biology*, *119*(4), 410–420. https://doi.org/10.1111/j.1744-7410.2000.tb00111.x

Schneider, C. A., Rasband, W. S., & Eliceiri, K. W. (2012). NIH Image to ImageJ: 25 years of image analysis. *Nature Methods*, *9*(7), 671–675. https://doi.org/10.1038/nmeth.2089

Schwalb-Willmann, J. (2024). *basemaps: Accessing Spatial Basemaps in R* (R package version 0.0.6) [Computer software]. https://CRAN.R-project.org/package=basemaps

Sköld, M., Josefson, A., & Loo, L.-O. (2001). Sigmoidal growth in the brittle star *Amphiura filiformis* (Echinodermata: Ophiuroidea). *Marine Biology*, *139*, 519–526. https://doi.org/10.1007/s002270100600

Stewart, B. G., & Mladenov, P. V. (1997). Population structure, growth and recruitment of the euryalinid brittle-star *Astrobrachion constrictum* (Echinodermata: Ophiuroidea) in Doubtful Sound, Fiordland, New Zealand. *Marine Biology*, *127*(4), 687–697. https://doi.org/10.1007/s002270050059

Stöhr, S., O'Hara, T. D., & Thuy, B. (2012). Global Diversity of Brittle Stars (Echinodermata: Ophiuroidea). *PLOS ONE*, *7*(3), e31940. https://doi.org/10.1371/journal.pone.0031940

Stratanenko, E. A. (2021). A Comparative Analysis of the Growth and Lifespan of *Ophiacantha bidentata* Retzius 1805 (Echinodermata, Ophiuroidea) in the High Latitudes of the Russian Arctic. *Biology Bulletin*, *48*(8), 1263–1271. https://doi.org/10.1134/S1062359021080276

Stratanenko, E. A., & Denisenko, S. G. (2020). Growth of *Stegophiura nodosa* (Echinodermata, Ophiuroidea) in the Pechora Sea. *Journal of the Marine Biological Association of the United Kingdom*, *100*(7), 1129–1133. https://doi.org/10.1017/S0025315420001010

Stump, R. J. W., & Lucas, J. S. (1990). Linear growth in spines from *Acanthaster planci* (L.) involving growth lines and periodic pigment bands. *Coral Reefs*, *9*(3), 149–154. https://doi.org/10.1007/BF00258227

Sun, J., Hamel, J.-F., Gianasi, B. L., & Mercier, A. (2019). Age determination in echinoderms: First evidence of annual growth rings in holothuroids. *Proceedings: Biological Sciences*, *286*(1906), 1–8.

TUNU - Biodiversity and Ecology of NE Greenland biota. UiT The Arctic University of Norway - Arctic Marine System Ecology (AMSE). Retrieved 11 May 2024, from https://uit.no/research/arcticmarinesystemecology/project?pid=819350&p_document_id=808639

Udalov, A. A., Vedenin, A. A., & Chava, A. I. (2018). Benthic Fauna of Stepovoi Bay (Novaya Zemlya Archipelago, Kara Sea). *Oceanology (Washington. 1965)*, *58*(6), 838–846. https://doi.org/10.1134/S0001437018060140

Vihtakari, M. (2024). *ggOceanMaps: Plot Data on Oceanographic Maps using 'ggplot2'* (R package version 2.2.0) [Computer software]. https://CRAN.R-project.org/package=ggOceanMaps

Whitfield, R. P. (1898). *Notice of a remarkable specimen of the West India coral Madrepora palmata. Bulletin of the AMNH ; v. 10, article 19.* http://hdl.handle.net/2246/763

Wickham, H. (2016). *ggplot2: Elegant Graphics for Data Analysis*. Springer-Verlag New York. https://ggplot2.tidyverse.org

Wickham, H., François, R., Henry, L., Müller, K., & Vaughan, D. (2023). *dplyr: A Grammar of Data Manipulation* (R package version 1.1.4) [Computer software]. https://CRAN.R-project.org/package=dplyr

Wilke, C. O. (2024). *cowplot: Streamlined Plot Theme and Plot Annotations for 'ggplot2'* (R package version 1.1.3) [Computer software]. https://CRAN.R-project.org/package=cowplot

Yokoyama, L. Q., & Amaral, A. C. Z. (2011). Recruitment and growth variation of *Ophionereis reticulata* (Echinodermata: Ophiuroidea). *Invertebrate Reproduction & Development*, *55*(2), 73–81. https://doi.org/10.1080/07924259.2011.553402

Yunda-Guarin, G., Michel, L., Nozais, C., & Archambault, P. (2022). Interspecific differences in feeding selectivity shape isotopic niche structure of three ophiuroids in the Arctic Ocean. *Marine Ecology. Progress Series*, *683*. https://doi.org/10.3354/meps13965

Zhulay, I., Iken, K., Renaud, P. E., & Bluhm, B. A. (2019). Epifaunal communities across marine landscapes of the deep Chukchi Borderland (Pacific Arctic). *Deep-Sea Research Part I, 151*. https://doi.org/10.1016/j.dsr.2019.06.011

Appendix